Molecular Therapy
Original Article

Tweaking lentiviral vector design balances efficacy and safety in liver-directed gene therapy for familial hypercholesterolemia

Cesare Canepari,[1,2] Michela Milani,[1] Sara Degl'Innocenti,[1] Marco Monti,[1] Monica Volpin,[1] Francesco Starinieri,[1,2] Maurizio Cavallo,[1] Anna Fabiano,[1] Mauro Biffi,[1] Marialucia Longo,[1] Fabio Russo,[1] Leonardo Ormoli,[1] Francesco Gazzo,[1,3] Rossana Norata,[1] Martina Rocchi,[4] Chiara Brombin,[5] Federica Cugnata,[5] Patrizia Cristofori,[1] Stefano Beretta,[1] Eugenio Montini,[1] Francesca Sanvito,[4] and Alessio Cantore[1,2]

[1]San Raffaele Telethon Institute for Gene Therapy, IRCCS San Raffaele Scientific Institute, 20132 Milan, Italy; [2]Vita-Salute San Raffaele University, 20132 Milan, Italy; [3]Department of Electronics, Information and Bioengineering, Politecnico di Milano, 20133 Milan, Italy; [4]IRCCS San Raffaele Scientific Institute, 20132 Milan, Italy; [5]Center for Statistics in the Biomedical Sciences, Vita-Salute San Raffaele University, 20132 Milan, Italy

Elevated low-density lipoprotein (LDL) cholesterol is the hallmark of familial hypercholesterolemia (FH), an inherited disease mostly due to mutations in the LDL receptor (LDLR)-encoding gene. Here, we enforced overexpression of LDLR in hepatocytes by *in vivo* lentiviral vector (LV) gene therapy and normalized circulating LDL cholesterol in a mouse model of FH. One year after gene therapy, we detected a high incidence of hepatic tumors in treated mice. Analysis of LV genomic integration sites in the liver tumors revealed expanded clones bearing LV insertions within the Fyn-related kinase (*Frk*) gene, a known hepatic oncogene, inducing the formation of aberrant *Ldlr-Frk* transcripts. When we purposely overexpressed LDLR-FRK by LV gene transfer, we observed hepatocellular hyperplasia and hypertrophy, supporting a role of this chimeric protein in oncogenesis. Since high expression of this chimeric oncogene and the LDLR likely cooperated to cause liver toxicity, we reduced the strength of LDLR expression within LV. We achieved normalization of circulating LDL cholesterol in two FH mouse models and prevention of atherosclerosis, even under high-fat diet challenge, without any long-term liver tumorigenicity. Overall, our in-depth assessment of the efficacy and safety of *in vivo* gene therapy for FH provides new insights into mechanisms of action and potential vulnerabilities, with implications for future developments of lipid-lowering gene therapies.

INTRODUCTION

Cardiovascular diseases are the leading cause of global mortality, with low-density lipoprotein cholesterol (LDL-c) as a major risk factor.[1] LDL is primarily cleared from the circulation by the LDL receptor (LDLR), which is mainly expressed by hepatocytes. Mutations in LDLR account for >90% of cases of familial hypercholesterolemia (FH), an inherited autosomal dominant metabolic disorder.[2,3] The remaining cases are due to missense mutations in apolipoprotein B (ApoB), a structural component of LDL that interacts with LDLR (5%–9% of cases),[4] or gain-of-function (GOF) mutations (<1% of cases) in proprotein convertase subtilisin kexin 9 (PCSK9), a negative modulator of LDLR.[5] These mutations lead to elevated LDL-c levels and progressive atherosclerosis.

The frequency of heterozygous FH is 1:220 individuals, while the most severe form, homozygous FH (Ho-FH), accounts for 1:300,000.[6] Ideally, circulating LDL-c should be <100 mg/dL (<2.5 mmol/L). In heterozygous patients, it is >200 mg/dL (>5 mmol/L). Compared to normal individuals, heterozygous untreated patients have a 50% increased risk of cardiovascular disease by age 50 for men and a 30% increased risk by age 60 for women. In HoFH patients, circulating LDL-c is >400 mg/dL (10 mmol/L). HoFH patients display atherosclerosis in childhood, cardiovascular disease within the first 2 decades of life, and myocardial infarction and death before 30 years of age, if left untreated. Another typical manifestation of ongoing cholesterol accumulation is the presence of xanthomas and xanthelasmas in the skin.[1]

Several treatments are available for people affected by FH, targeting different components of cholesterol and lipid metabolism. Such treatments include statins, monoclonal antibodies (mAb), or short-interfering RNAs against PCSK9 and mAb against angiopoietin-like 3 (ANGPTL3).[7] These treatments, however, have limitations such as adverse effects, partial efficacy, and the need for repeated administrations. As such, there remains a significant unmet clinical need. In particular, HoFH patients, who exhibit the most severe phenotype and require multiple lipid-lowering medications and invasive LDL apheresis, can still fail to reach target LDL-c levels.[1]

Received 14 October 2025; accepted 12 December 2025;
https://doi.org/10.1016/j.ymthe.2025.12.036.

Correspondence: Alessio Cantore, San Raffaele Telethon Institute for Gene Therapy, IRCCS San Raffaele Scientific Institute, 20132 Milan, Italy.
E-mail: cantore.alessio@hsr.it

Please cite this article in press as: Canepari et al., Tweaking lentiviral vector design balances efficacy and safety in liver-directed gene therapy for familial hypercholesterolemia, Molecular Therapy (2025), https://doi.org/10.1016/j.ymthe.2025.12.036

Gene therapy offers the prospect of a one-time treatment for FH and potentially for more common forms of hypercholesterolemia. A single intravenous (i.v.) administration of a vector encoding LDLR might be sufficient to increase LDLR expression in hepatocytes, the primary cells responsible for LDL-c clearance. Among viral vectors, adeno-associated viral vectors (AAVs) are the most advanced for *in vivo* liver-directed gene therapy, with products already available for adults with hemophilia.[8,9] AAV-mediated LDLR gene therapy for the treatment of FH showed promising results in pre-clinical models,[10–13] and an early clinical trial for adults with FH was started. However, due to a lack of efficacy, the trial was discontinued (NCT02651675). Moreover, AAVs are mainly episomal, and thus remain extrachromosomal in the nucleus of target cells. This feature can limit their long-term efficacy following hepatocyte proliferation during liver growth and turnover, representing a particular challenge for pediatric patients who would benefit the most from a gene therapy approach for FH.

In contrast to AAV, lentiviral vectors (LVs) integrate into the genome of target cells. As a result, they may represent a suitable option for long-lasting *in vivo* gene therapy in pediatric patients. In line with this, we and others showed long-term persistence of transgene expression by hepatocytes, following *in vivo* administration of LV-containing hepatocyte-specific expression cassettes in neonatal and adult mice and in large animal models.[14–17] Extensive safety studies found no genotoxic events from LV-mediated liver gene transfer, despite the semi-random genomic integration pattern of the LV.[14,18] In the context of FH, a challenge with LV production is that the vesicular stomatitis virus glycoprotein (VSV.G), which is commonly used as a surface protein pseudotype to confer high infectivity and stability, uses LDLR and its family members as receptors. This interaction complicates the vector production of VSV.G-pseudotyped LDLR-encoding LV because overexpression of LDLR reduces yield.[19,20] Previously described LDLR-expressing LVs were associated with low infectious titers,[21,22] and administration of LDLR LV in FH disease models resulted in low efficacy.[23,24]

Here, we report an in-depth assessment of the efficacy, durability, and safety of *in vivo* LDLR gene therapy in mouse models of FH by LV. We describe stepwise refinement of LV design to solve issues encountered throughout our study, including minimal LV productivity and liver toxicity, with implications also for other gene therapy strategies. These advancements eventually enabled full long-term normalization of LDL-c and prevention of atherosclerosis, with both standard and cholesterol-/fat-enriched diets, without liver tumorigenicity, by *in vivo* LV gene therapy.

RESULTS

Abrogating LDLR overexpression in LV-producer cells rescues the yield of LDLR-expressing LV and allows effective *in vivo* gene therapy of FH

We first generated LV constructs expressing the wild-type (WT) version of the human LDLR cDNA under the control of a previously described hepatocyte-specific expression cassette, based on the strong chimeric enhanced transthyretin (ET) promoter (ET-hLDLR).[14] We observed a major >10-fold drop in infectious titer, physical particles, and infectivity of human LDLR-expressing LV, compared to GFP-expressing LV, used as control (Figures 1A–1C). These data suggest that overexpression of the LDLR within LV-producer cells caused detrimental interactions between the receptor and VSV.G during LV biogenesis and/or re-infection of the producer cells by the produced LV, resulting in the accumulation of LV inside producer cells at the expense of LV in the supernatant. LDLR overexpression was due to the activity of the ubiquitous promoter driving expression of LV genomic RNA in producer cells, despite the presence of the hepatocyte-specific internal promoter (Figure 1D).[25–27] LDLR-expressing LV displayed an infectious titer lower than what is required for *in vivo* LV administration to mice at doses needed for effective liver gene transfer, based on our previous experience.[15] Thus, to avoid the co-expression of VSV.G and LDLR during LV production, we produced LDLR-expressing LV using baculovirus-derived glycoprotein 64 (GP64) surface protein as LV pseudotype,[28] in place of VSV.G. While we confirmed the drop in infectious titer, physical particles, and infectivity of VSV.G-pseudotyped LDLR-expressing LV, we observed similar productivity of GP64-pseudotyped LV, whether LDLR was used as a transgene or the control human factor IX transgene (Figures 1E–1G). These data confirm that the decrease in productivity observed with VSV.G-pseudotyped LDLR-expressing LV was due to an interaction between VSV.G and LDLR, in line with previous reports.[21,22] However, since VSV.G-pseudotyped LVs transduce hepatocytes at higher efficiency than GP64-pseudotyped LV following *in vivo* administration to mice,[29] we aimed at rescuing the productivity of VSV.G-pseudotyped LV, by avoiding LDLR overexpression during LV production. To this end, we inverted the orientation of the transgene expression cassette, turning it into antisense (AS) orientation compared to LV genome transcription (Figure 1H). By this *escamotage*, we completely rescued the productivity of LDLR-expressing VSV.G-pseudotyped LV (Figures 1I–1K).

We then transduced human and mouse hepatoma cell lines with LV expressing LDLR either in the canonical sense orientation or AS orientation. We observed slightly lower expression of LDLR when placed in AS orientation, at matched LV doses and transduction as determined by LV DNA copies per diploid genomes (vector copy number, VCN; Figures S1A–S1F). Having solved the productivity issue, we moved to *in vivo* experiments in *Ldlr*$^{-/-}$ mice, a model of FH. We expected the entry of VSV.G-pseudotyped LV into hepatocytes and subsequent gene transfer to be allowed by the presence of LDLR family members, despite the absence of LDLR itself.[17] However, it was previously shown that the murine LDLR transgene is more effective than a human transgene in reducing LDL-c in mice, after AAV gene therapy,[30] due to a more efficient binding of the murine LDLR with the murine LDL structural components. For this reason, we generated and produced LV expressing the murine LDLR (mLDLR) in AS orientation, since mLDLR expressing LV in sense orientation resulted in very low infectious titer, recapitulating what we observed with LV expressing the human LDLR (Figure S1G).

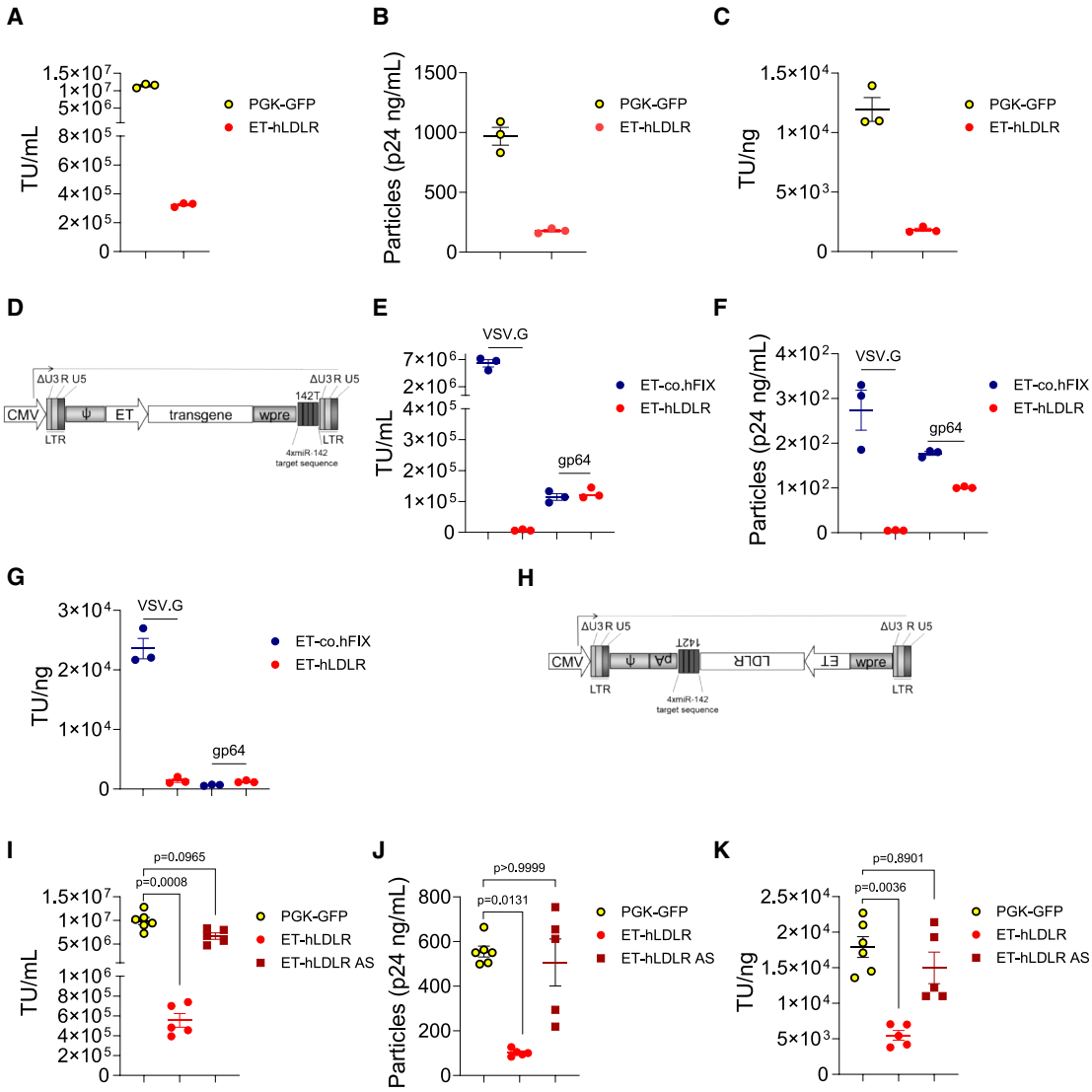

Figure 1. Productivity of LDLR-encoding LV

(A) Single values and mean with standard error of the mean (SEM) of infectious titer of non-concentrated LV encoding GFP or hLDLR, as indicated. (B and C) Single values and mean with SEM of LV particles (ng HIV Gag p24/mL; B) or specific infectivity (TU/ng p24; C) of non-concentrated LV encoding GFP or hLDLR as indicated, titered on 293T cells. (D) Schematic representation of the self-inactivating (SIN) LV transfer plasmid with the transgene cassette in the same orientation as the LV genome. CMV, cytomegalovirus promoter/enhancer, required for LV genome transcription during LV production; ΔU3, deletion of the promoter/enhancer of the HIV long terminal repeats (LTRs); the poly(A) signal-containing R and the U5 regions of the LTR are retained; ψ, packaging signal; strong hepatocyte-specific enhanced transthyretin (ET) promoter composed of synthetic hepatocyte-specific enhancers and transthyretin promoter; wpre, mutated woodchuck hepatitis virus posttranscriptional regulatory element[25,26]; 142T, microRNA-142 target sequence made of 4 tandem copies of a sequence perfectly complementary to microRNA 142, expressed by hematopoietic cells. The addition of 142T eliminates off-target transgene expression in hematopoietic lineages.[27] (E–G) Single values and mean with SEM of infectious titer (E), LV particles (F) or specific infectivity (G) of non-concentrated LV encoding FIX or hLDLR, pseudotyped with VSV.G (left part of each panel), or GP64 (right part of each panel), as indicated, titered on 293T cells. (H) Schematic representation of the SIN LV transfer plasmid with the transgene cassette in AS orientation relative to the LV genome. By this design, expression of the transgene product is avoided in LV-producer cells during LV production, but it occurs in LV-transduced hepatocytes, where the ET promoter is active. pA, poly(A) signal of the bovine growth hormone gene. (I) Single values and mean with SEM of infectious titer of non-concentrated LV encoding GFP, hLDLR, or antisense-oriented (AS) hLDLR, as indicated. Pool of two independent experiments. Kruskal-Wallis test with Dunn's multiple comparisons test. (J and K) Single values and mean with SEM of LV particles (J) or specific infectivity (K) of non-concentrated LV encoding GFP, hLDLR, or AS hLDLR, as indicated, titered on 293T cells.

Please cite this article in press as: Canepari et al., Tweaking lentiviral vector design balances efficacy and safety in liver-directed gene therapy for familial hypercholesterolemia, Molecular Therapy (2025), https://doi.org/10.1016/j.ymthe.2025.12.036

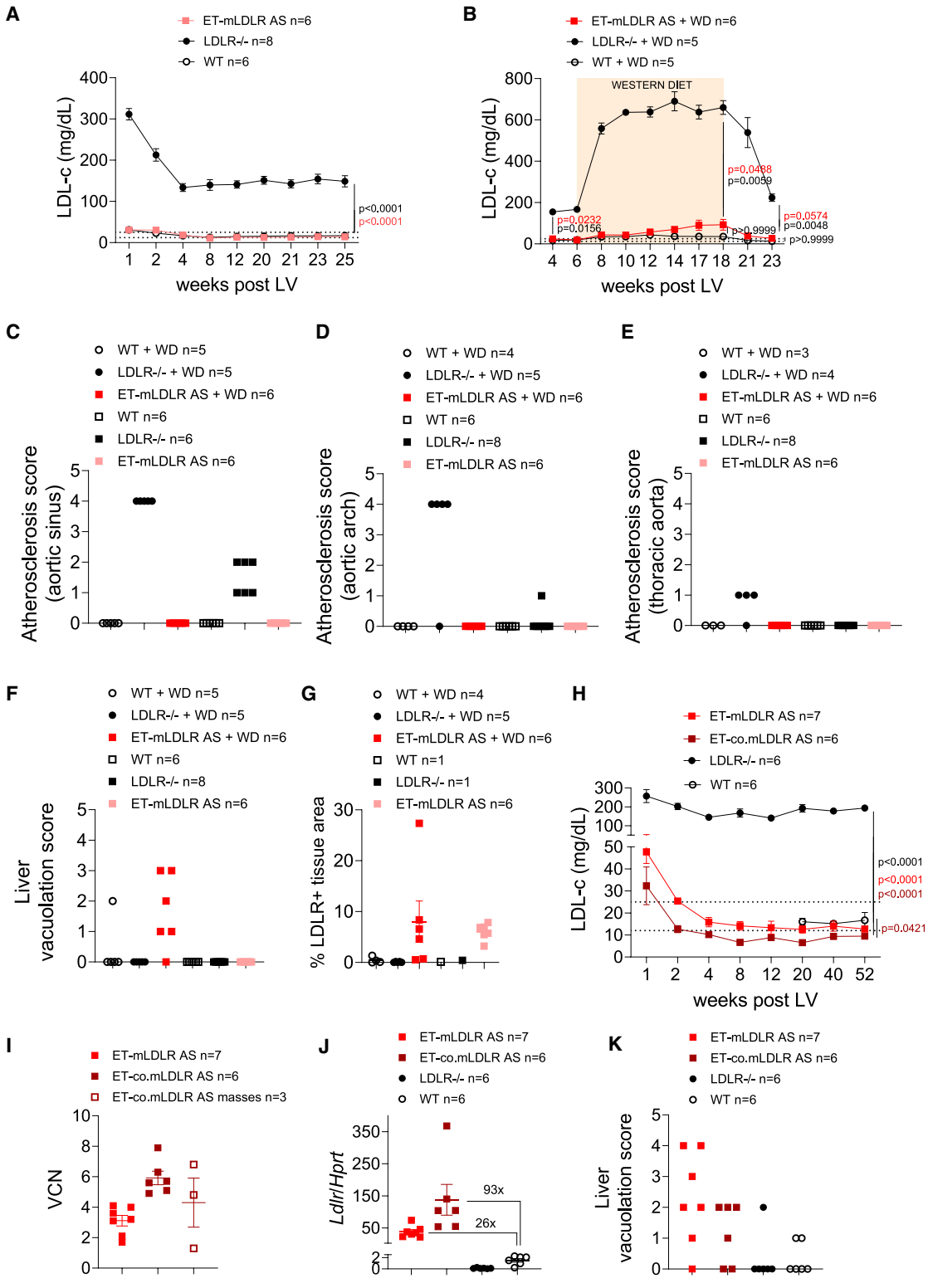

(legend on next page)

Please cite this article in press as: Canepari et al., Tweaking lentiviral vector design balances efficacy and safety in liver-directed gene therapy for familial hypercholesterolemia, Molecular Therapy (2025), https://doi.org/10.1016/j.ymthe.2025.12.036

Treatment for FH patients should start promptly after diagnosis to prevent progressive atherosclerosis. For this reason, we treated the mice as juveniles (2 weeks old), by i.v. delivery of 4×10^{10} transducing units (TU)/kg of ET-mLDLR LV AS. We observed full normalization of LDL-c and total cholesterol in gene therapy-treated mice compared to untreated *Ldlr*$^{-/-}$ controls, with a remarkable 10-fold LDL-c reduction, maintained throughout the 6 months of follow-up (Figures 2A and S1H). Untreated *Ldlr*$^{-/-}$ controls showed an initial spontaneous decline in LDL-c and total cholesterol, possibly due to the dietary change following weaning. Atherosclerosis does not extensively develop in *Ldlr*$^{-/-}$ mouse model unless the mice are challenged with a high-fat, high-cholesterol diet, referred to as Western diet (WD).[31] To assess if LV-treated mice were protected from atherosclerosis, we thus repeated the experiment including a WD challenge. We treated juvenile *Ldlr*$^{-/-}$ mice with ET-mLDLR LV at 4×10^{10} TU/kg and confirmed LDL-c normalization in the first weeks following gene therapy (Figures 2B and S1I). Then, we fed the mice with WD for 3 months, before returning to the standard chow diet. During the WD challenge, *Ldlr*$^{-/-}$ untreated controls showed a very pronounced increase in LDL-c and total cholesterol, with a clearly visible lipemic serum (Figure S1J). By contrast, LV-treated mice resisted the challenge similarly to normal mice, and LDL-c was reduced again upon WD discontinuation (see Figures 2B and S1I). Six months after LV administration and 1.5 months after discontinuing WD, we closed the experiment and performed histopathological analysis of aortas and livers on the mice of this and of the previous experiment. We detected atherosclerosis in all *Ldlr*$^{-/-}$ mice fed with WD and in some *Ldlr*$^{-/-}$ mice fed with a standard diet, at the level of the aortic sinus, arch, and thoracic aorta, and we scored it in accordance to severity (Figures 2C–2E; S2A). Atherosclerosis was absent in WT mice as well as in all gene therapy-treated *Ldlr*$^{-/-}$ mice, fed with either chow or WD. In the liver, we found that ET-mLDLR-LV-treated mice fed with WD showed higher hepatocellular vacuolation than all the other groups (Figure 2F). However, none of the ET-mLDLR-LV-treated mice showed any hepatocellular vacuolation when kept on a normal diet (Figures 2F and S2B). We then evaluated the percentage of liver area positive for LDLR (LDLR+) by immune fluorescence analysis and found variable LDLR+ area among LV-treated mice (Figure 2G). Interestingly, we observed that the higher the severity score of hepatocellular vacuolation, the lower the LDLR+ area, suggesting intrahepatic lipid accumulation in the case of a few LV-corrected hepatocytes (Figure S2C; Table S3). Overall, these data show that LV gene therapy to hepatocytes resulted in full normalization of LDL-c and prevention of atherosclerosis in FH mice, enabled by high infectivity of LDLR-expressing LV and efficiency of gene transfer.

Long-term monitoring of mice treated with LDLR-overexpressing LV reveals liver toxicity

Next, we assessed the long-term durability and safety of liver gene therapy using the WT or a codon-optimized mLDLR transgene. We confirmed long-term stable normalization of circulating LDL-c and total cholesterol in juvenile *Ldlr*$^{-/-}$ mice treated with ET-mLDLR or ET-co.mLDLR LV, without a significant advantage conferred by the use of the codon-optimized transgene (Figures 2H and S3A). We followed LV-treated mice for 1 year. We found macroscopic masses in the livers of some LV-treated mice at necropsy. LV VCN on the total liver ranged from 1.7 to 7.9 (Figure 2I), indicating an efficient LV transduction of the liver in *Ldlr*$^{-/-}$ mice. The liver masses were LV positive as well (Figure 2I). We measured *Ldlr* RNA and observed a considerably higher *Ldlr* expression in the livers of LV-treated mice, compared to the physiological *Ldlr* of healthy counterparts (26- to 93-fold), indicating massive *Ldlr* overexpression in the LV-transduced livers (Figure 2J). Histopathological evaluation showed vacuolation of hepatocytes with increased incidence and severity score in LV-treated mice, compared to WT and *Ldlr*$^{-/-}$ controls (Figure 2K). Moreover, histopathological evaluation diagnosed the macroscopic masses as adenomas and detected additional microscopic adenomas not visible at necropsy (Figure S3B). Overall, liver adenomas occurred in 54% of LV-treated mice (Figure S3C). In addition, preneoplastic changes, i.e., foci of cellular alteration, were present in two out of seven mice treated with ET-mLDLR LV. Age-matched untreated *Ldlr*$^{-/-}$ and WT controls did not show proliferative changes (Figure S3C). This high incidence of tumor formation in LV-treated mice was unexpected since we did not observe any tumorigenicity in previous studies of *in vivo* LV gene therapy.[14,15,18] We thus hypothesized that the newly tested AS configuration could contribute to the observed outcome. Indeed, in this LV design, enhancer sequences in the ET promoter localize close to the mutated woodchuck hepatitis virus posttranscriptional regulatory element (wpre), used in LV to improve infectious titer.[25,26] It has been shown that the wpre

Figure 2. Long-term efficacy and safety of ET-LDLR LV AS

(A) Mean with SEM of serum LDL-c in *Ldlr*$^{-/-}$ mice treated with ET-mLDLR LV AS (4×10^{10} TU/kg) when 2 weeks old, at the indicated time post LV, or in age-matched untreated WT or *Ldlr*$^{-/-}$ mice, as indicated. The dotted line shows WT mice LDL-c normal range (12–25 mg/dL). Linear-mixed effects (LME) model (only p values <0.05 are reported; for complete analyses, see Table S1). (B) Mean with SEM of serum LDL-c in *Ldlr*$^{-/-}$ mice treated with ET-mLDLR LV AS (4×10^{10} TU/kg) when 2 weeks old, at the indicated time post LV, or in age-matched untreated WT or *Ldlr*$^{-/-}$ mice, as indicated. From 9 weeks of age (7 weeks post LV), all the mice started a 3-month-long WD challenge (highlighted area) and then returned to a standard chow diet until the end of the follow-up. Kruskal-Wallis test with Dunn's multiple comparisons test at the indicated time points. (C–E) Atherosclerosis score (see materials and methods) of mice in (A) and (B) at the level of aortic sinus (C), aortic arch (D), or thoracic aorta (E). (F) Hepatocellular lipid vacuolation score (see materials and methods) of mice in (A) and (B). (G) Single values and mean with SEM of the percentage of LDLR-positive liver area in mice in (A) and (B). (H) Mean with SEM of serum LDL-c in *Ldlr*$^{-/-}$ mice treated with ET-mLDLR LV AS (5×10^{10} TU/kg) or ET-co.mLDLR LV AS (1×10^{11} TU/kg) when 2 weeks old at the indicated time post LV, or in age-matched untreated WT or *Ldlr*$^{-/-}$ mice, as indicated. LME model on the last three time points (only p values <0.05 are reported; for complete analyses, see Table S4). (I) Single values and mean with SEM of VCN measured in the total liver of mice in (H). (J) Single values and mean with SEM of *Ldlr* expression, normalized on the endogenous *Hprt* gene, in the livers of mice in (H). (K) Hepatocellular lipid vacuolation score of mice in (H).

Please cite this article in press as: Canepari et al., Tweaking lentiviral vector design balances efficacy and safety in liver-directed gene therapy for familial hypercholesterolemia, Molecular Therapy (2025), https://doi.org/10.1016/j.ymthe.2025.12.036

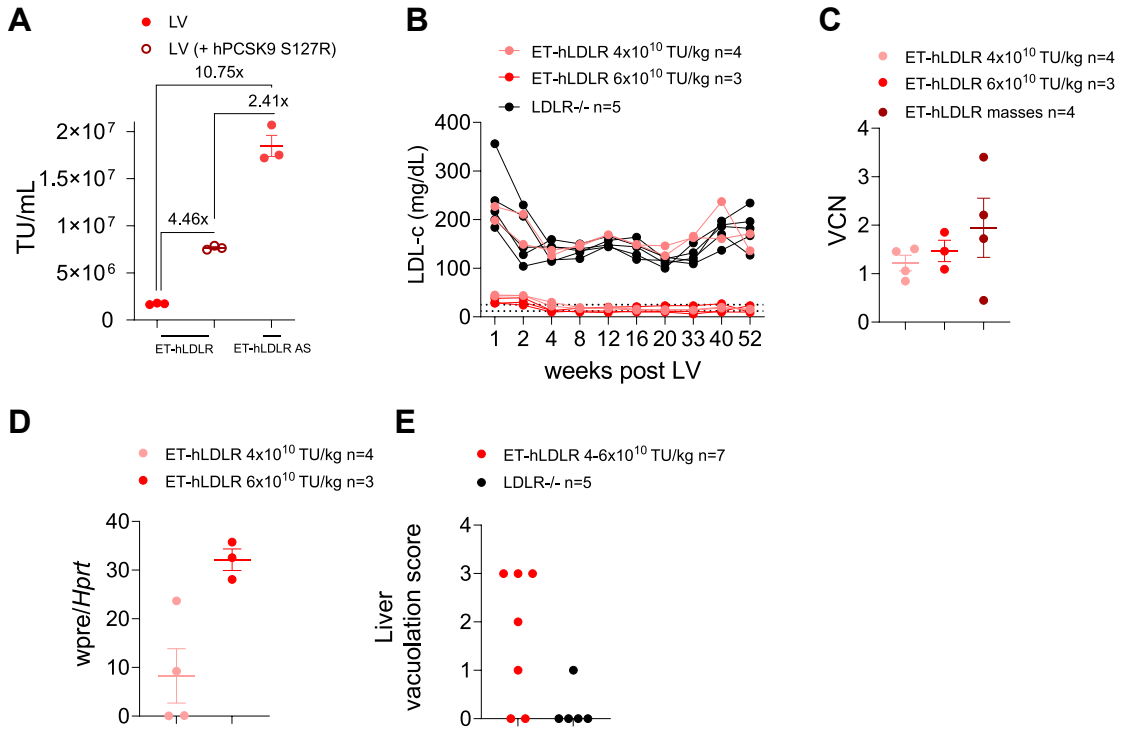

Figure 3. Productivity, long-term efficacy, and safety of ET-LDLR LV

(A) Single values and mean with SEM of infectious titer of non-concentrated LV encoding hLDLR or hLDLR AS, produced with or without human PCSK9 S127R, as indicated. (B) Single values of serum LDL-c in *Ldlr*$^{-/-}$ mice treated with ET-hLDLR LV (4 or 6 × 10^{10} TU/kg), when 2 weeks old, at the indicated time post LV, or in age-matched untreated *Ldlr*$^{-/-}$ mice as indicated. (C) Single values and mean with SEM of VCN measured in the total liver of mice in (B). (D) Single values and mean with SEM of wpre expression (proxy of LV transgene), normalized on the endogenous *Hprt* gene, in the livers of mice in (B). (E) Hepatocellular lipid vacuolation score of mice in (B).

contains a promoter, so the AS LV configuration may activate oncogenes downstream of the LV integration site by enhancing wpre-mediated transcription (Figure S3D).[25,26]

This consideration prompted us to return to the canonical sense-oriented LV design, used in our previous studies.[14,15,18] To do so, we exploited PCSK9, the natural negative modulator of LDLR, reasoning that expressing PCSK9 during LV production may force degradation of LDLR before its exposure on the membrane of the cells, thus reducing the interaction between LDLR and VSV.G and the re-infection of producer cells by the LV released in the supernatant (Figure S4A). To maximize LDLR degradation and avoid carryover in the LV preparation, we used a non-secreted GOF human PCSK9 variant (S127R) causing FH, more powerful than WT PCSK9.[32] When we produced LV expressing human LDLR in sense orientation, we achieved a remarkable 4.5-fold higher infectious titer in the presence of human PCSK9-S127R, despite not reaching the titer of AS-oriented LV design (Figure 3A). Nevertheless, the LV titer obtained was sufficient to move to the *in vivo* experiment. We used the human transgene to ensure interaction with the human PCSK9-S127R.

We thus treated juvenile *Ldlr*$^{-/-}$ mice with ET-hLDLR both at the dose used in the previous experiments employing mLDLR (4 × 10^{10} TU/kg), and at a higher dose (6 × 10^{10} TU/kg), expecting a lower binding efficiency of the hLDLR to mouse LDL structural components. All the mice in the high-dose group showed normalization of LDL-c and total cholesterol (Figures 3B and S4B), maintained for 1 year. Still, we found macroscopic masses in the livers of some LV-treated mice at necropsy (57%). LV was detectable in the masses' DNA (Figure 3C). Again, we observed supranormal transgene RNA expression in LV-treated mice compared to WT controls (compare Figure 3D with Figure 2J). Histopathology analysis of the livers showed vacuolation of hepatocytes with increased incidence and severity score in LV-treated mice, compared to *Ldlr*$^{-/-}$ controls. The masses were diagnosed as hepatocellular adenomas (Figures 3E and S4C). The two mice without liver vacuolation were those without detectable LDL-c reduction, suggesting a lack of efficient hepatocyte transduction (see Figures 3B and 3E). Taken together, these data show that LV gene therapy to hepatocytes resulted in long-term LDL-c normalization; however, it caused liver toxicity, independently of the orientation of the LDLR expression cassette within the LV.

LV integrations within the Fyn-related kinase *Frk* gene, shared among liver tumors, generate aberrant *Ldlr-Frk* fusion transcripts

To assess the possible role of LV-mediated insertional mutagenesis in the observed outcome, we performed high-throughput LV integration site (IS) analysis on all the macroscopically normal livers

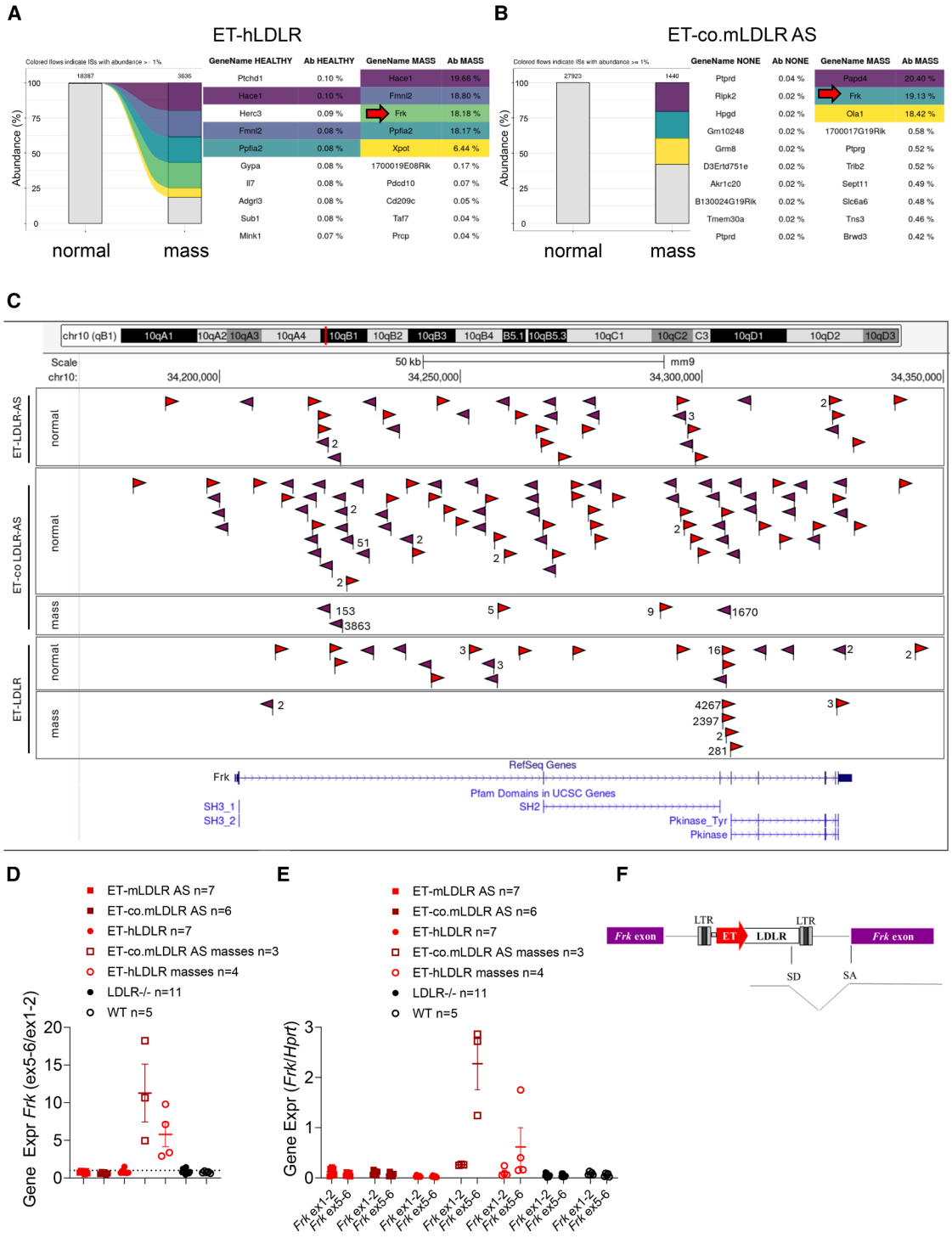

Figure 4. LV genomic IS analysis of macroscopically normal livers and liver masses

(A and B) Stacked bar plots representing the abundance of each LV IS retrieved from the liver of a representative mouse treated with the LV construct shown on top. The left bars show macroscopically normal livers, and the right bars show the liver mass. Colored stacks indicate ISs with a relative abundance >1%. Light gray bars represent all the ISs with <1% abundance. The total number of ISs retrieved is shown on the top of the bar. The reference gene of the top 10 most abundant ISs and their relative percentage are shown in the list on the right. (C) Genomic position of LV ISs within *Frk* in the normal livers of ET-mLDLR AS (first rectangle), ET-co.mLDLR AS (second rectangle), or ET-LDLR (fourth rectangle). The third and fifth rectangles indicate LV ISs within *Frk* in the masses of ET-co.mLDLR AS or ET-hLDLR, respectively. The chromosome number and

(legend continued on next page)

Please cite this article in press as: Canepari et al., Tweaking lentiviral vector design balances efficacy and safety in liver-directed gene therapy for familial hypercholesterolemia, Molecular Therapy (2025), https://doi.org/10.1016/j.ymthe.2025.12.036

and liver masses of LV-treated mice followed for 1 year. We retrieved a considerably higher number of unique LV ISs from the liver tissues than from the isolated masses (Figure S5A), without any dominant clone in the former (Figures S5B–S5N). Conversely, we found an oligoclonal LV IS profile in the masses, with dominant clones characterized by the high relative abundance of unique ISs (Figures 4A, 4B, and S6A–S6E). This finding was further supported by a clonal diversity decrease in the masses, as shown by a reduced Shannon Diversity Index, compared to the non-tumoral livers (Figures S6F–S6H). These data suggest a polyclonal pattern of integration of LV at the time of administration, maintained for 1 year of follow-up in normal livers, and that one or a few hepatocyte clones in which LV integrated in specific genomic loci progressively expanded, ultimately leading to overt tumor formation, in some mice. In the masses, we found recurrent ISs in introns 1 or 3 of the *Frk* gene, a non-receptor tyrosine kinase, known to be involved in hepatic oncogenesis,[33,34] likely implying a causal role of these LV insertions in tumor development. The presence of other abundant ISs is compatible with expanded clones transduced at multiple LV copies. To understand a possible mechanism of insertional mutagenesis, we focused on the orientations of LV insertions within this gene. In the liver tissues of LV-treated mice, where ISs in *Frk* accounted for very low genome counts, approximately 50% of the integrations were in the same orientation of *Frk* transcription, and 50% in the opposite direction, as expected by the unbiased orientation of LV genomic integration.[35,36] By contrast, within the masses, 100% of the dominant clones displayed integrated LDLR transgenes in the same orientation of *Frk* transcription (Figure 4C), a hallmark of a "promoter insertion" genotoxicity mechanism.[35]

To investigate this phenomenon, we measured *Frk* mRNA upstream and downstream of LV ISs in the macroscopically normal livers and the liver masses. While in the former, both regions of *Frk* were similarly expressed, in all the masses, we observed higher amounts of *Frk* RNA downstream than upstream of the LV ISs (Figures 4D and 4E), suggesting that the ET promoter inside the LV upregulated the downstream portion of *Frk*. To confirm this hypothesis, we evaluated the presence of aberrant transcripts comprising part of the *Ldlr* transgene and part of *Frk*. We detected such transcripts in the liver masses (Figure S7A), and sequencing confirmed a fusion open reading frame comprising most of the *Ldlr* linked in-frame to the first available exon of *Frk* following each LV IS (Figures S7B–S7D). This result suggests the occurrence of a splicing event in the terminal portion of the LDLR transgene (Figure 4F), leading to a fusion mRNA likely translated into a chimeric protein encompassing the LDLR extracellular and transmembrane domains fused to the kinase domain of FRK. This mRNA was expressed at higher levels than normal *Frk*, due to the superior activity of the ET promoter compared to the endogenous *Frk* promoter (see Figures 4D and 4E). Overall, these data indicate that LV insertions within the *Frk* gene contributed to hepatic tumorigenesis through a "promoter insertion" mechanism of insertional mutagenesis, which led to an overexpressed chimeric *Ldlr-Frk* mRNA, likely inducing hepatocyte proliferation and clonal expansions, predisposing to tumor formation.

Transcriptomic analysis of the liver tumors shows upregulation of FRK-related proliferative signaling pathways

To analyze the global gene expression profile of the livers of treated mice and of liver tumors, we performed transcriptomic analysis of histologically normal liver samples from LV-treated or untreated $Ldlr^{-/-}$ mice and of six of the liver tumors found in LV-treated mice, as described above.

The highest number of differentially expressed genes (DEGs) with a false discovery rate (FDR) <0.05 and absolute log fold change [abs(logFC)] >0.5 was detected when comparing the tumor samples with normal livers from either LV-treated or untreated $Ldlr^{-/-}$ mice (12,756 and 9,175, respectively), indicating a remarkably different transcriptome of the liver tumors (Figures 5A and 5B). When comparing liver samples of untreated $Ldlr^{-/-}$ mice and WT mice, we detected 487 DEGs, likely due to the defective LDLR function (Figure 5C). Interestingly, LV-treated livers showed fewer DEGs when compared to those of WT mice (134) than compared to those of untreated mice (618), suggesting reshaping of the transcriptome toward that of WT mice by the LV treatment (Figures 5D and 5E). Dysregulated pathways between WT and $Ldlr^{-/-}$ mice comprised inflammatory response and cholesterol homeostasis, a phenotype likely due to the missing LDLR (Figures 5F and 5G). Among pathways positively enriched in tumors compared to the normal livers of either LV-treated or untreated $Ldlr^{-/-}$ mice, we found typical cancer-related processes, such as mitotic spindle, KRAS signaling, epithelial to mesenchymal transition, and angiogenesis. Interestingly, STAT signaling was also upregulated, consistent with a known

the coordinates of *Frk* are indicated on top, while the *Frk* gene is depicted underneath, with its 8 exons indicated as small vertical bars. Each flag indicates the presence and the location of LV genomes retrieved within *Frk*. The number next to each flag indicates genome counts retrieved in the *Frk* locus among different experimental normal livers and liver masses. Exclusively, numbers corresponding to genome counts >1 are annotated in the figure; all the other flags correspond to a genome count = 1. Red flags indicate LV genomes integrated in the same orientation, and purple flags indicate LV genomes integrated in opposite orientations relative to *Frk* transcription. In case of sense-oriented LV, LDLR sequence is in the same orientation of the LV genome. In the case of AS LV, the LDLR sequence is in the opposite orientation to the LV genome. Please note that in 100% of dominant integrations within the masses, the LDLR transgene is in the same orientation as *Frk* transcription. (D) Single values and mean with SEM of the ratio between *Frk* expression at the exon 5–6 junction (ex5-6) and at the exon 1–2 junction (ex1-2) in the normal livers and masses, as indicated. (E) Single values and mean with SEM of *Frk* expression normalized on the endogenous *Hprt* gene, at the level of exon 1–2 or exon 5-6 junctions, in the normal livers and masses, as indicated. (F) Schematic representation of the mechanism of genotoxicity, likely occurring in liver tumors: the ET promoter drives robust expression of LDLR, sometimes splicing into the first available *Frk* exon downstream the LV IS, through cryptic splice donor sites in LDLR, leading to the generation of a chimeric transcript comprising part of *Ldlr* and part of *Frk*.

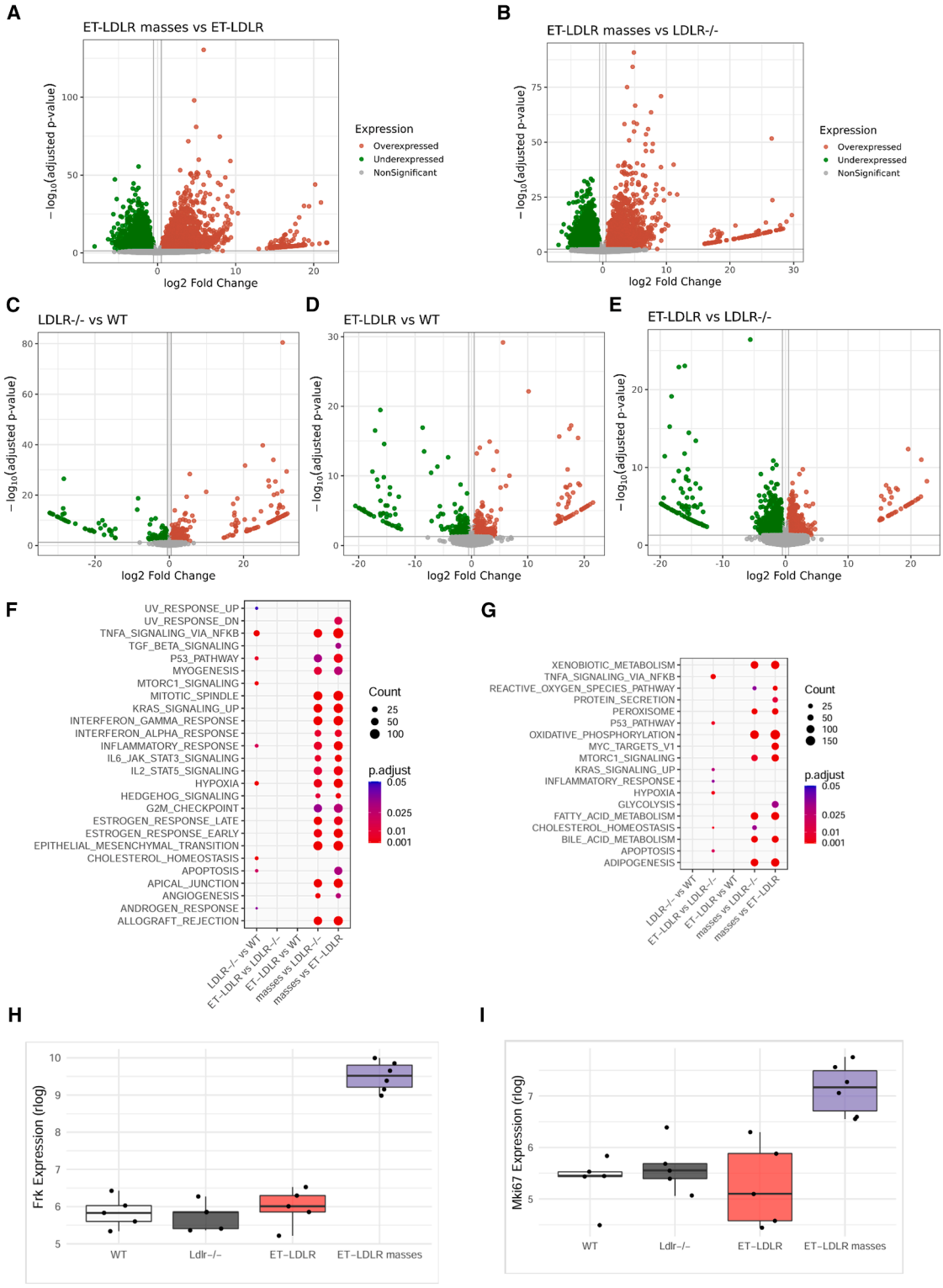

Figure 5. RNA sequencing of macroscopically normal livers and liver tumors

(A–E) Volcano plots of differentially expressed genes (DEGs) across indicated comparisons. (A) Tumor vs. normal livers in LV-treated mice. (B) Tumor vs. normal livers in untreated *Ldlr*$^{-/-}$ mice. (C) *Ldlr*$^{-/-}$ vs. WT livers. (D) LV-treated vs. WT livers. (E) LV-treated vs. *Ldlr*$^{-/-}$ livers. Genes with $|\log_2 FC| > 0.5$ and adjusted $p < 0.05$ are considered

(legend continued on next page)

Please cite this article in press as: Canepari et al., Tweaking lentiviral vector design balances efficacy and safety in liver-directed gene therapy for familial hypercholesterolemia, Molecular Therapy (2025), https://doi.org/10.1016/j.ymthe.2025.12.036

downstream effect of *Frk* hyperactivation.[34] Among pathways negatively regulated in the tumors, we observed those typical of hepatocyte identity, such as xenobiotic, fatty acid, and bile acid metabolism, suggesting partial loss of differentiation within the tumoral samples (see Figures 5G and 5F). We confirmed high expression of *Frk* and also observed high *Mki67* expression in liver tumors, supporting the expected proliferative state (Figures 5H and 5I).

Expression of an LDLR-FRK chimeric protein causes hepatomegaly and hepatocellular hyperplasia

To further confirm that the expression of a chimeric LDLR-FRK protein was detrimental, and the driver of the observed tumorigenicity, we generated an LV encoding the chimeric LDLR-FRK protein observed in one of the retrieved adenomas, resulting from the translation of the aberrant mRNA consisting of most of the co.mLDLR joined to *Frk* cDNA encompassing exons 2–8 (Figure S8A). We then treated juvenile WT and $Ldlr^{-/-}$ mice with this LDLR-FRK-expressing LV at 3–4 $\times$ 10^{10} TU/kg. A few weeks after LV administration, most LV-treated mice displayed a swollen abdomen, and the experiment was terminated when they started showing reduced activity, i.e., 2 months post LV for WT mice or 1 month post LV for $Ldlr^{-/-}$ mice. At necropsy, the livers of LV-treated mice showed hepatomegaly with areas of discoloration, in contrast to macroscopically healthy livers of untreated mice (Figure S8B). The mean weight of the liver of treated mice accounted for 15%–18% of the total weight of the mouse, compared to only 4% in control mice (Figure 6A). The liver VCN between the two strains was comparable (Figure 6B). Histopathological evaluation of the liver showed vacuolation of hepatocytes in all treated mice, albeit with different severity scores (Figures 6C and S8C). None of the controls showed hepatocellular vacuolation. All LV-treated mice showed hyperplastic hepatocytes, and most of them showed various grades of hepatocellular hypertrophy, compared to none of the controls (Figures 6D and S8C–S8E). Several livers were immunolabeled with Ki67, confirming that the proliferation rate was higher in LV-treated mice (Figures 6E, S8D, and S8E). Taken together, these data provide evidence on the detrimental and pro-proliferative effects induced by the massive overexpression of the chimeric protein comprising most of LDLR and an FRK sequence deprived of part of its auto-inhibitory domain (present in exon 1). Overall, these data support a major role of *Ldlr-Frk* aberrant transcripts in promoting the observed tumorigenicity in LV-treated mice.

Moderate LDLR expression corrects FH without long-term liver tumorigenicity

We then aimed at avoiding the long-term genotoxicity due to ET-LDLR treatment. We reckoned that the strength of the ET promoter may be unnecessary in the context of FH, based on the *Ldlr* RNA data (see Figure 2J). Therefore, we tested a basal hepatocyte-specific human alpha-1-antitrypsin (HAAT) promoter, characterized by a weaker expression than the ET promoter. We kept the LV design AS oriented with the HAAT promoter, to ensure high productivity (Figure S9A). When tested *in vitro* in a hepatoma cell line, LV with the HAAT promoter expressed *Ldlr* ~20-fold less than LV with the ET promoter at matched LV doses (Figures S9B–S9D).

Interestingly, when tested *in vivo* in juvenile $Ldlr^{-/-}$ mice, we found similar therapeutic efficacy of LV equipped with the two promoters at similar LV doses, 5–6 $\times$ 10^{10} TU/kg (Figures 7A and S9E). The HAAT-driven *Ldlr* expression was significantly lower than when ET-driven, in the livers of treated mice, at comparable VCN (Figures 7B and 7C). Having defined the feasibility of using HAAT-LDLR LV in a short-term experiment, we treated additional $Ldlr^{-/-}$ mice with ET-mLDLR LV (3 $\times$ 10^{10} TU/kg) and HAAT-mLDLR LV (4 $\times$ 10^{10} TU/kg) in parallel and followed them for 1 year. We confirmed the reduction of circulating LDL-c and total cholesterol, stably maintained throughout the follow-up (Figures 7D and S9F). We did not find macroscopic masses in any liver of LV-treated mice at necropsy. We observed lower liver VCN in ET-mLDLR-treated mice compared to the HAAT-mLDLR LV group (Figure 7E), in line with the administered LV doses. Histopathological evaluation confirmed the livers of LV-treated mice to be devoid of any evidence of microscopic adenomas (Figure S9G). Absence of adenomas in the ET-mLDLR LV group in this experiment was likely due to the lower dose used, resulting in a lower integration rate, compared to the previous one (compare Figures 2I and 7E). The frequency of liver vacuolation was higher in LV-treated mice compared to controls (Figures 7F and S9H). We performed oil red O staining, confirming that vacuolation was due to lipid accumulation (Figure S9I). Comparing the livers of mice treated with the two different constructs, treatment with ET-mLDLR LV resulted in a more pronounced microvesicular vacuolation of hepatocytes, associated with a higher incidence of necrotic foci with aggregates of pigmented, foamy macrophages (Figures 7G and S9J).

To corroborate efficacy and lack of long-term liver tumorigenicity with this novel HAAT-LDLR LV design, we treated an additional cohort of juvenile $Ldlr^{-/-}$ mice at therapeutic doses (4 or 6 $\times$ 10^{10} TU/kg). We followed them for 1 year. At both LV doses, we detected normal circulating LDL-c and total cholesterol (Figures 7H and S10A), with up to 10-fold LDL-c reduction compared to untreated $Ldlr^{-/-}$ mice. At the end of the experiment, we detected a liver VCN of 4 and 5.5 on average in the two dose groups (Figure 7I). Histopathology analysis confirmed the absence of any proliferative

significant; upregulated genes are shown in red, downregulated genes in green, and non-significant genes in gray. (F and G) Dot plot of enriched hallmark pathways upregulated (F) or downregulated (G) in each comparison between the first and second condition. The x axis indicates the comparisons, while the y axis shows the enriched pathways. Dot size reflects the number of genes (Count) that are significantly upregulated (F) or downregulated (G) in that particular pathway, while dot color indicates statistical significance (adjusted p value). Only pathways with adjusted p <0.05 are displayed. (H and I) Boxplot of the rlog normalized expression level of *Frk* (H) and *Mki67* (I) across all experimental conditions (n = 6 for the tumor condition, and n = 5 for all other conditions). Boxes represent the interquartile range, horizontal lines indicate medians, and individual points correspond to biological replicates.

Please cite this article in press as: Canepari et al., Tweaking lentiviral vector design balances efficacy and safety in liver-directed gene therapy for familial hypercholesterolemia, Molecular Therapy (2025), https://doi.org/10.1016/j.ymthe.2025.12.036

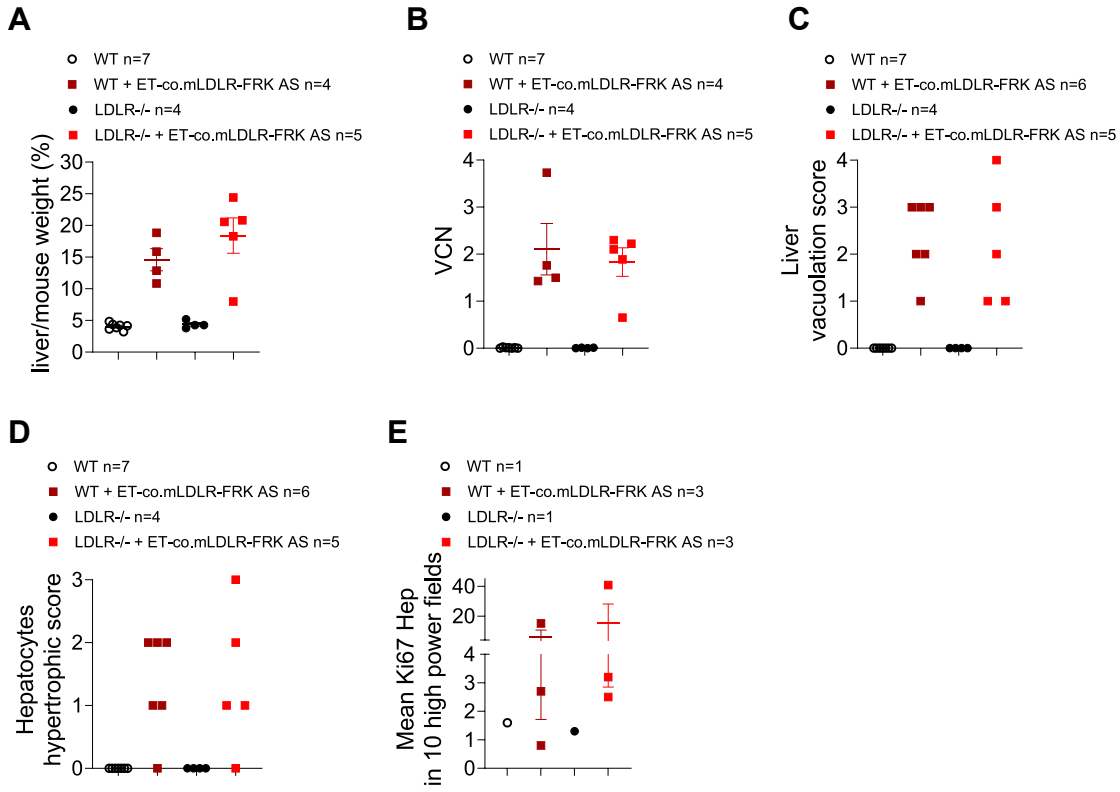

Figure 6. Gene transfer of LDLR-FRK in juvenile mice

(A) Mean and SEM of liver to mouse weight, expressed in percentage, of WT or *Ldlr*$^{-/-}$ mice, treated or not with LV encoding *Ldlr-Frk* fusion transcript. 2-week-old WT or *Ldlr*$^{-/-}$ mice were injected with 4×10^{10} TU/kg or 3×10^{10} TU/kg, respectively, and euthanized 2 months post LV (WT) or 1 month post LV (*Ldlr*$^{-/-}$). (B) Single values and mean with SEM of VCN measured in the total liver of mice in (A). (C) Hepatocellular lipid vacuolation score of mice in (A). Two additional WT LV-treated mice, found dead in the cage 1 week before the scheduled euthanasia, were analyzed at histopathology, although the liver was not weighed, and liver VCN was not performed. (D) Hepatocellular hypertrophic score of mice in (A). (E) Mean and SEM of the mean of proliferating (Ki67-positive) hepatocytes detected in 10 high-power fields (400×) per mouse. Mice were randomly selected among the ones in (A).

lesion in LV-treated mice (Figure S10B), and we did not detect any aberrant transcript comprising *Ldlr* and *Frk* (Figure S10C). Increased incidence of hepatocellular vacuolation was detected in LV-treated mice, compared to WT and *Ldlr*$^{-/-}$ control mice (Figure 7J). We performed high-throughput LV IS analysis on all livers from HAAT-LDLR LV-treated mice followed for 1 year. We detected a highly polyclonal pattern of LV integration, without any dominant clone (Figure S11), indicating a semi-random pattern of LV integration at the time of administration and absence of any clonal expansion, over time.

At this point, we tested whether HAAT-LDLR LV-treated mice could resist a WD challenge. We treated additional juvenile *Ldlr*$^{-/-}$ mice with HAAT-LDLR LV at 4×10^{10} TU/kg dose and confirmed normalization of LDL-c and total cholesterol during the first weeks post LV (Figures 7K and S12A). When fed with WD for 3 months, LV-treated mice resisted the challenge, while untreated *Ldlr*$^{-/-}$ mice showed the expected increase in both parameters. Once WD was discontinued, LDL-c and total cholesterol decreased again (see Figures 7K and S12A). At the end of the follow-up (6 months post LV), we detected marked atherosclerosis in *Ldlr*$^{-/-}$ age-matched controls (Figures 7L and S12B). Atherosclerosis was not observed in LV-treated mice, except for one mouse showing a few subendothelial foamy macrophages in the aortic sinus, scored as a grade 1. LV-treated mice did not show higher lipid vacuolation in the liver than normal age-matched controls (Figures 7M and S12C; Table S10). Overall, these data show that LV-mediated liver gene therapy with LDLR under the control of the HAAT promoter achieves therapeutic efficacy in the absence of long-term liver tumorigenicity.

The efficacy of liver gene therapy by HAAT-LDLR LV is confirmed in an FH mouse model recapitulating human LDL composition

In mice, in contrast to humans, ApoB, the structural component of LDL, is present both in its complete form (referred to as ApoB100, where 100 stands for 100% of ApoB) and in its truncated form (referred to as ApoB48, where 48 stands for 48% of ApoB). Indeed, murine hepatocytes post-transcriptionally edit ApoB, which results in a premature stop codon, truncating the protein prematurely.[37]

Please cite this article in press as: Canepari et al., Tweaking lentiviral vector design balances efficacy and safety in liver-directed gene therapy for familial hypercholesterolemia, Molecular Therapy (2025), https://doi.org/10.1016/j.ymthe.2025.12.036

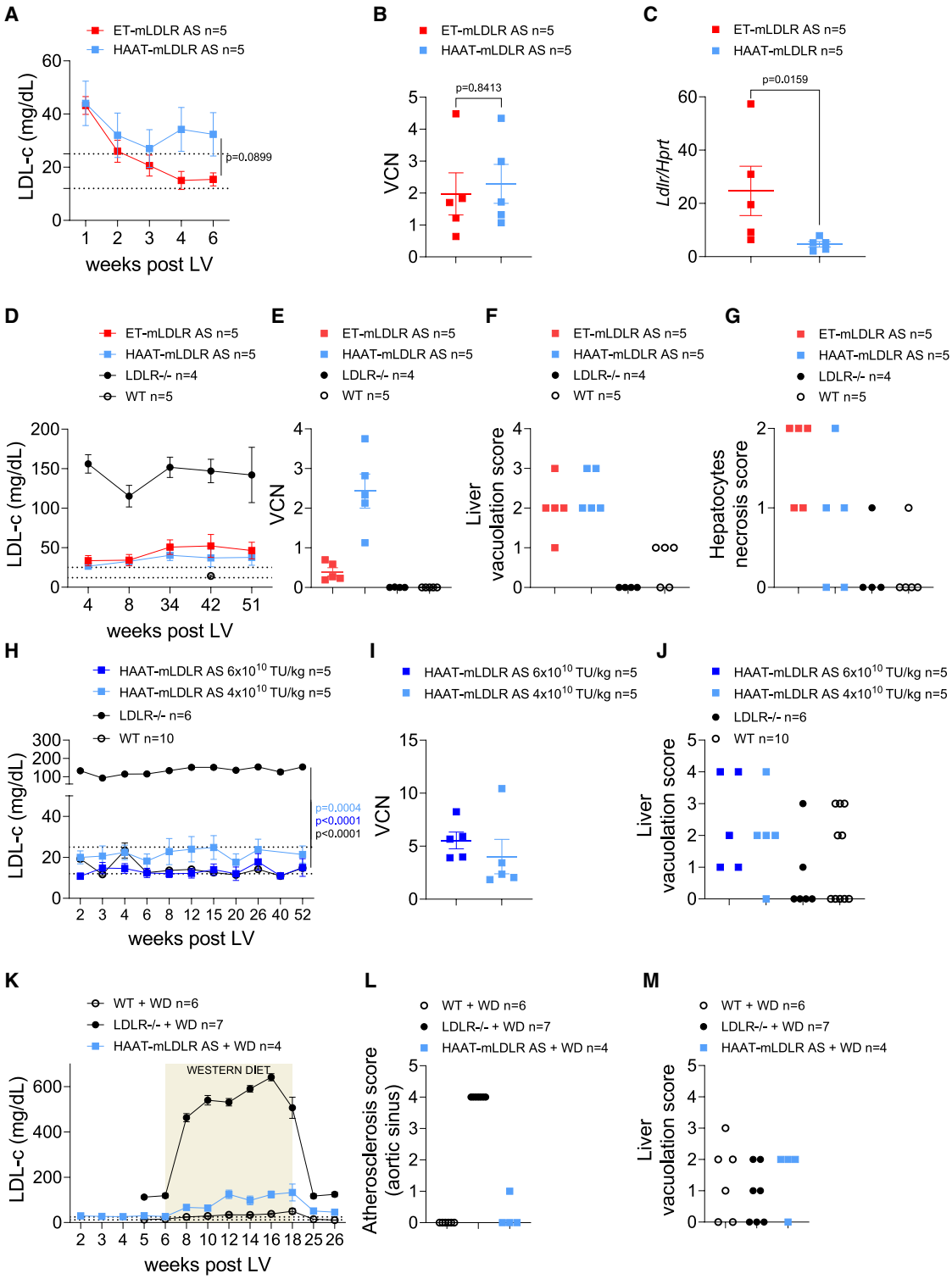

Figure 7. Long-term efficacy and safety of HAAT-LDLR LV AS

(A) Mean with SEM of serum LDL-c in *Ldlr*$^{-/-}$ mice treated with ET-mLDLR LV AS (6×10^{10} TU/kg) or HAAT-mLDLR LV AS (5×10^{10} TU/kg) when 2 weeks old at the indicated time post LV. LME model (only *p* values <0.05 are reported; for complete analyses, see Table S6). (B) Single values and mean with SEM of VCN measured in the total

(legend continued on next page)

LDL carrying ApoB48 can be captured by LDLR family members, in addition to LDLR itself, resulting in reduced half-life and representing one of the reasons for minimal-mild atherosclerosis of the *Ldlr*$^{-/-}$ mouse model, when fed with a standard diet. In order to further assess the efficacy potential of the described gene therapy with LV HAAT-LDLR, we treated *Ldlr*$^{-/-}$ mice expressing exclusively ApoB100, which recapitulate the human LDL composition.[37] We treated *ApoB100-Ldlr*$^{-/-}$ juvenile mice by i.v. delivery of 6×10^{10} TU/kg of HAAT-mLDLR LV AS. We observed full normalization of LDL-c and total cholesterol in gene therapy-treated mice, even reaching hypocholesterolemic amounts, compared to untreated *ApoB100-Ldlr*$^{-/-}$ controls, with a 30-fold LDL-c reduction, maintained throughout the 3 months of follow-up (Figures 8A and S12D). Overall, these data reinforce the efficacy of LV HAAT-LDLR gene therapy and elect this vector design as the leading candidate for a possible gene therapy of FH.

DISCUSSION

In this study, we highlight the potential of *in vivo* liver-directed LV gene therapy for FH in mouse models, while addressing the challenges to reach long-term therapeutic efficacy and safety. We show that LDLR gene transfer to hepatocytes leads to a potent >10-fold reduction of LDL-c, normalizing levels in hypercholesterolemic mice treated as juveniles. This effect was maintained for up to 1 year, indicating the persistence of genetically corrected cells through liver growth and homeostatic renewal. To ensure efficient LDLR gene transfer to hepatocytes, we focused on improving the productivity rate of LDLR-expressing LV pseudotyped with VSV.G, an envelope protein known to transduce the liver efficiently following *in vivo* administration.[14,29] We successfully enhanced productivity by placing LDLR in an antisense orientation relative to LV genome transcription, preventing LDLR overexpression during LV production. This strategy may be applied to other transgenes, whose expression can be detrimental to vector production. We also tested the effects of forcing LDLR degradation during LV production by co-expressing an FH-associated mutated form of PCSK9, a natural negative modulator of LDLR. This strategy may also be applied in other settings, whenever an inhibitor of the transgene of interest is known.

In the context of FH, it is likely that supranormal LDLR transgene expression is required to achieve full therapeutic efficacy by *in vivo* gene therapy, since transducing all hepatocytes with current delivery systems is unfeasible[38] and because there would not be a selective advantage of the corrected cells over the non-corrected ones. Moreover, LDLR is normally expressed in other tissues beyond the liver, albeit at lower levels.[39] As such, even liver transplantation, the most effective treatment currently available for HoFH patients, is not sufficient to normalize LDL-c.[40] Genome editing approaches that aim to correct mutations in LDLR at its endogenous locus might not suffice as a single treatment, similar to liver transplantation. Base editing techniques that target LDLR mutations[41,42] are challenging due to the high number (>2000) of known pathogenic variants.[43] By contrast, base editing or epigenetic silencing to reduce PCSK9 expression[44,45] shows promise to reduce LDL-c and is currently being tested in early-stage clinical trials.[46] This approach, however, will only be relevant to heterozygous FH patients who carry a functional copy of LDLR. Alternatively, base editing to reduce ANGPTL3 expression might be suitable for HoFH patients, with an expected 45%–50% reduction in LDL-c.[7] This level of reduction, however, would likely be insufficient to bring LDL-c to target levels in this patient population.

By contrast, *in vivo* LV-LDLR gene therapy could potentially be administered to all FH patients early in life, ensuring lifelong LDL-c normalization and atherosclerosis prevention. Liver-directed *in vivo* gene therapy indeed has the potential to reach full efficacy, as LDLR expression can be modulated according to the promoter used within the vector construct. When using a strong hepatocyte-specific ET enhancer/promoter, we achieved >25-fold higher *Ldlr* expression than normal, normalizing blood cholesterol. However, we detected a high incidence of hepatic tumors in treated mice, 1 year post LV. This phenomenon was not observed in previous studies using the same LV design but with different transgenes, such as coagulation factors.[15,18] This differential outcome suggests that it is LDLR overexpression in *Ldlr*$^{-/-}$ hepatocytes that contributes to LV-induced tumorigenesis. Insertional mutagenesis occurred independently of the LDLR transgene sequences and cassette orientation but was dependent on the promoter used. Interestingly, in mice treated with LDLR LV under the control of the strong ET promoter, adenoma formation was LV-dose dependent. These results suggest that LV-mediated genotoxicity is modulated by the genetic elements present within the LV construct (promoter sequences),[35,47] is linked to the disease context (LDLR overexpression in *Ldlr*$^{-/-}$ mice), emerges over the long term (1 year after LV administration), and is dependent on the LV dose. These findings highlight the importance of long-term pre-clinical safety assessments of gene therapies in disease models.

liver of mice in (A). (C) Single values and mean with SEM of transgene-derived *Ldlr* expression, normalized on the endogenous *Hprt* gene, in the livers of mice in (A). (D) Mean with SEM of serum LDL-c in *Ldlr*$^{-/-}$ mice treated with ET-mLDLR LV AS (3×10^{10} TU/kg) or HAAT-mLDLR LV AS (4×10^{10} TU/kg) when 2 weeks old at the indicated time post LV. (E) Single values and mean with SEM of VCN measured in the total liver of mice in (D). (F) Hepatocellular lipid vacuolation score of mice in (D). (G) Hepatocellular necrosis score of mice in (D). (H) Mean with SEM of serum LDL-c in *Ldlr*$^{-/-}$ mice treated with HAAT-mLDLR LV AS ($4–6 \times 10^{10}$ TU/kg) when 2 weeks old at the indicated time post LV or in age-matched untreated WT or *Ldlr*$^{-/-}$ mice, as indicated. LME model (only p values <0.05 are reported; for complete analyses, see Table S8). (I) Single values and mean with SEM of VCN measured in the total liver of mice in (H). (J) Hepatocellular lipid vacuolation score of mice in (H). (K) Mean with SEM of serum LDL-c in *Ldlr*$^{-/-}$ mice treated with HAAT-mLDLR LV AS (4×10^{10} TU/kg) when 2 weeks old at the indicated time post LV or in age-matched untreated WT (C57) or *Ldlr*$^{-/-}$ mice, as indicated. From 9 weeks of age (7 weeks post LV), all the mice started a 3-month-long WD challenge (highlighted area) and then returned to a standard chow diet until the end of the follow-up. (L) Atherosclerosis score (see materials and methods) of mice in (K) at the level of aortic sinus. (M) Hepatocellular lipid vacuolation score of mice in (K).

Please cite this article in press as: Canepari et al., Tweaking lentiviral vector design balances efficacy and safety in liver-directed gene therapy for familial hypercholesterolemia, Molecular Therapy (2025), https://doi.org/10.1016/j.ymthe.2025.12.036

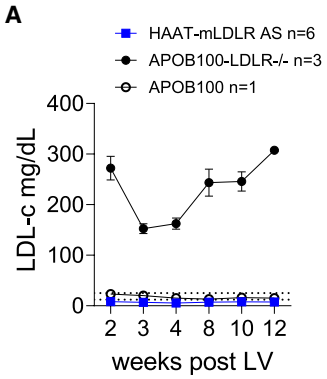

Figure 8. Efficacy of HAAT-LDLR AS in a humanized mouse model

(A) Mean with SEM of serum LDL-c in *ApoB100-Ldlr*$^{-/-}$ mice treated with HAAT-mLDLR LV AS (6×10^{10} TU/kg) when 2 weeks old at the indicated time post LV.

Mechanistically, we found that long-term LV-mediated insertional mutagenesis with ET-LDLR constructs led to the formation of aberrant *Ldlr-Frk* fusion transcripts. The mechanism involved splicing into the downstream portion of the gene targeted by the IS, suggesting that the presence of cryptic splicing donor sites in the LV transgene should be avoided. A chimeric LDLR-FRK receptor present on the hepatocyte cell membrane might respond to extracellular amounts of LDL and provide pro-proliferative signals intracellularly through its kinase domain; such altered signaling could lead to tumor formation in LV-treated mice. In-frame fusion genes comprising *Frk* have been identified both in hepatocellular and hematological malignancies, and the deletion of the SH2/SH3 domain, together with an intact tyrosine kinase domain, is known to be critical for the oncogenic mechanism of *Frk* fusions.[34] RNA sequencing of liver tumors confirmed that *Frk* was among the most upregulated genes compared to other conditions. Moreover, within the tumors, JAK-STAT, belonging to the FRK signaling pathway,[34] was among the upregulated pathways compared to healthy livers from LV-treated mice. Mice treated with LDLR-FRK LV manifested hepatomegaly, along with hyperplastic and hypertrophic hepatocytes, and showed an increased hepatocyte proliferative index, supporting a role of this chimeric protein in tumorigenicity. In the mice treated with LDLR LV, 1 year was required for the clone carrying the detrimental LV integration to expand and give rise to an adenoma. Conversely, all hepatocytes transduced with LDLR-FRK-LV expressed the chimeric protein, anticipating the onset of manifestations to 1–2 months post LV. It is worth noting that mice treated with LDLR-FRK-LV also showed a high rate of hepatocellular vacuolation, short term, suggesting a role of FRK, once dysregulated, in promoting liver steatosis. Indeed, FRK has been recently associated with both total and LDL cholesterol traits,[48] and cases of adenomas due to uncontrolled FRK overexpression were associated with liver steatosis.[49]

When we expressed LDLR transgene to levels slightly higher than normal using the basal HAAT promoter, we achieved full efficacy without tumorigenicity over the long term in *Ldlr*$^{-/-}$ mice. This result indicates that despite an initial similar integration pattern by the two LV constructs, the high expression mediated by the ET promoter of the LDLR transgene and, consequently, of the *Ldlr-Frk* aberrant transcript, aggravated genotoxicity in a dose-dependent manner. At a lower dose, ET-LDLR treatment did not show detectable tumorigenicity, yet it resulted in near-normal circulating LDL-c amounts, suggesting that the effective and toxic doses may be too close to provide a comfortable therapeutic window for clinical translation. By contrast, our findings support a larger therapeutic window by the HAAT-LDLR LV, which enabled full efficacy without detectable genotoxicity. Notably, *Ldlr-Frk* fusion transcripts were not detected in mice treated by the HAAT-LDLR LV. In line with our findings, recent reports have highlighted remarkably different outcomes in patients receiving LV-mediated *ex vivo* hematopoietic stem cell gene therapy, with insertional oncogenesis emerging exclusively when using a strong retroviral promoter in the LV construct.[50,51] Diseases like FH, where achieving gene transfer in a large proportion of hepatocytes is more relevant than overexpressing too much of the transgene per cell, may be the right candidate to test weak hepatocyte-specific promoters to drive the transgene of interest. Importantly, using HAAT-LDLR LV, efficacy was also reached when treating a mouse model more closely recapitulating the human condition, where LDL carries exclusively ApoB100 as a structural component.

Over the long term, we observed hepatocellular vacuolation in LV-treated mice, comparable between the two promoters, suggesting that LDLR overexpression can predispose to liver steatosis. Excessive LDLR expression may lead to uncontrolled uptake of lipid-containing lipoproteins and/or retention of newly synthesized ones. Indeed, *Ldlr*$^{-/-}$ hepatocytes can synthesize the necessary cholesterol autonomously,[2] while LDLR-overexpressing hepatocytes might become overloaded with lipids.[52] Although the degree of hepatocellular vacuolation was comparable between the two promoters, ET-LDLR-treated mice showed a more pronounced microvesicular vacuolation of hepatocytes, associated with higher inflammation. These data indicate that reducing the extent of LDLR overexpression ameliorates the liver condition. When challenging both HAAT-LDLR LV-treated mice and WT controls with a WD, the two groups displayed a comparable amount of vacuolation. It should be noted that the *Ldlr*$^{-/-}$ mouse model might overestimate the risk of liver steatosis following LDLR gene therapy. For example, people carrying GOF LDLR variants leading to lifelong LDL-c levels that are 74% lower than normal do not display liver steatosis.[53] Moreover, mice lacking PCSK9 are predisposed to develop liver steatosis compared to WT mice, while humans with hypocholesterolemia due to LOF PCSK9 mutations are not.[54] These data suggest that mild LDLR hepatic overexpression is unlikely to predispose patients to steatosis.

In conclusion, we present an LV-based gene therapy strategy for FH with pre-clinical proof of concept demonstrating unprecedented efficacy and good tolerability. By addressing productivity and toxicity concerns, we have transformed an initially unfeasible LV design into an efficient LDLR-expressing LV without detectable tumorigenic risk. Additional pre-clinical investigation of LV in AS configuration,

Please cite this article in press as: Canepari et al., Tweaking lentiviral vector design balances efficacy and safety in liver-directed gene therapy for familial hypercholesterolemia, Molecular Therapy (2025), https://doi.org/10.1016/j.ymthe.2025.12.036

expressing LDLR under a mild hepato-specific promoter in other animal models, e.g., the spontaneous FH rabbit model, is now a warranted step toward clinical translation. If proven effective and safe by further pre-clinical studies and potential clinical trials, this therapy could be potentially considered for acquired forms of hypercholesterolemia.

MATERIALS AND METHODS

Study design

Sample size in experiments with mice was chosen according to previous experience with experimental models and assays. No sample or animal was excluded from the analyses. Mice were randomly assigned to each experimental group. Investigators were not blinded.

Plasmid construction

The plasmids used for this work were already available in the lab, or they were generated through standard cloning techniques, inserting into available backbones inserts derived from other pre-existing plasmids or derived from gene synthesis required ad hoc. *LDLR* cDNA sequences were synthetized through GenScript, based on the sequence available online (NCBI>CCDS Database). *Ldlr* cDNA sequences were synthesized through GenScript based on the sequence available online (NCBI>CCDS Database). Codon optimization was performed by GenScript, for mice. The cDNA sequence of hPCSK9 S127R was synthesized through GenScript. The ET promoter can be found at GenBank: AY661265. The HAAT promoter has the following sequence: gatcttgctaccagtggaacagccactaaggattctgcagtgagagcagagggccagctaagtggtactctcccagagactgtctgactcacgccacccccctccaccttggacacaggacgctgtggtttctgagccaggtacaatgactccttttcggtaagtgcagtggaagctgtacactgcccaggcaaagcgtccgggcagcgtaggcgggcgactcagatcccagccagtggacttagcccctgtttgctcctccgataactggggtgaccttggttaatattcaccagcagcctccccgttgcccctctggatccactgcttaaatacggacgaggacag.

Plasmid DNA purification

Large-scale amounts of plasmids DNA, required during vector generation, were obtained using Machaery-Nagel-endotoxin-free high-purity plasmid maxi preparation system. Purification was performed following the manufacturer's instructions. Plasmids were resuspended in TE (10 mM Tris-HCl, pH 8, 1 mM EDTA). Nature Technology Corporation generated the packaging plasmid and the envelope plasmid. Small-scale amounts of plasmids DNA, required during the screening of colonies following cloning, were obtained using Wizard Plus SV Minipreps DNA Purification System (Promega).

Vector production

Third-generation self-inactivating (SIN) LVs were produced by calcium phosphate transient transfection into 293T cells. The cells were transfected with a solution containing a mix of the selected LV genome transfer plasmid, the packaging plasmids pMDLg/pRRE and pCMV.REV, pMD2.G, and pAdVantage (Promega), as previously described.[14] In case of further addition of *PCSK9* plasmid (pMax.*PCSK9*), its amount per plate was 15 μg. Briefly, the medium was changed 14–16 h after transfection, and the supernatant was collected 30 h after the medium change. LV-containing supernatants were sterilized through a 0.22-μm filter (Millipore), transferred into sterile polyallomer tubes (Beckman), and centrifuged at 20,000 × g for 120 min at 20°C (Beckman Optima XL-100K Ultracentrifuge). The LV pellet was dissolved in the appropriate volume of PBS to allow 500–1000X concentration. In the experiments in which LDLR-LV productivity was tested, plasmid amounts were the following: pMDL/RRE, 5 μg/plate; pCMV.REV, 2.5 μg/plate; PMD2.VSV.G or pBA.AcMNPV.gp64, 4 μg/plate; pAdvantage plasmid, 7.5 μg/plate; and transfer plasmid, 15 μg/plate. In case of further addition of *PCSK9* plasmid, its amount per plate was 7.5 μg. The collection was performed 30 h post transfection. In this context, titrations were performed on the non-concentrated cell supernatant.

LV titration

For LV titration, 1×10^5 293T cells were transduced with serial LV dilutions in the presence of polybrene (8 μg/mL). Genomic DNA (gDNA) was extracted 14 days after transduction, using Maxwell 16 Cell DNA Purification Kit (Promega), following the manufacturer's instructions. VCN was determined by droplet digital PCR (ddPCR), starting from 5 to 20 ng of template gDNA using primers (HIV fw: 5′-T ACTGACGCTCTCGCACC-3'; HIV rv: 5′-TCTCGA CGCAGGACTCG-3′) and a probe (FAM 5′-ATCTCTCTCCTTC TAGCCTC-3′) designed on the primer binding site region of LV. The amount of endogenous DNA was quantified by a primers/probe set on the human telomerase gene (Telo fw: 5′-GGCACACGTG GCTTTTCG-3'; Telo rv: 5′-GGTGAACCTCGTAAGTTTATGC AA-3'; Telo probe: VIC 5′-TCAGGACGTCGAGTGGACACGG TG-3′ TAMRA) or the human GAPDH gene (Applied Biosystems HS00483111_cm). The PCR reaction was performed with each primer (900 nM) and the probe (250 nM, 500nM for Telo) following the manufacturer's instructions (Bio-Rad), read with QX200 reader, and analyzed with QuantaSoft software (Bio-Rad). Infectious titer, expressed as TU/mL, was calculated using the formula TU/mL = (VCNx100,000x(1/dilution factor)). LV physical particles were measured by HIV-1 Gag p24 antigen immunocapture assay (PerkinElmer) following the manufacturer's instructions. LV-specific infectivity was calculated as the ratio between infectious titer and physical particles.

VCN determination

DNA was extracted from whole liver samples using Maxwell 16 Tissue DNA Purification Kit (Promega) for mouse experiments. VCN in murine DNA line was determined by ddPCR, starting from 5 to 20 ng of template gDNA using a primers/probe set designed on the primer binding site region of LV (see LV titration above). The amount of endogenous DNA was quantified by a primers set designed on the human telomerase gene, as above, or the murine Sema3A gene, as described below. The amount of endogenous murine DNA was quantified by a primers/probe set designed on the murine sema3a gene (Sema3A fw: 5′-ACCGATTCCAGATGATTGGC-3'; Sema3A rv: 5′-TCCATATTAATGCAGTGCTTGC-3'; Sema3A probe: HEX 5′-AGAGGCCTGTCCTGCAGCTCATGG-3′ BHQ1). The PCR reaction was performed with each primer (900 nM,

150nM for RT-LV primers) and the probe (250 nM) following the manufacturer's instructions (Bio-Rad), read with QX200 reader, and analyzed with QuantaSoft software (Bio-Rad).

Cell cultures and *in vitro* experiments

293T cells were maintained in Iscove's modified Dulbecco's medium (IMDM, Gibco 21980-032) with additive L-glutamine, 25mM HEPES, penicillin and streptomycin 100 international units (IU)/mL (Lonza) and supplemented with 10% fetal bovine serum (FBS, FetalClone II, HyClone, Euroclone). All cells were maintained in a 5% CO_2 humidified atmosphere at 37°C. All cell lines were routinely tested for mycoplasma contamination. Huh7 or Hepa1.6 cell lines were transduced for 24 h and then cultured for 14 days before being analyzed by fluorescence-activated cell sorting. The gDNA was then extracted and VCN determined (see VCN determination).

Flow cytometry

Flow cytometry analyses were performed using a FACSCanto analyzer (BD Biosciences), equipped with DIVA Software, as previously described.[15] Around 500,000 Huh7 and Hepa1.6 cells were harvested and washed with PBS. Staining was conducted in MACS buffer, incubating Huh7 and Hepa1.6 cells with *hLDLR* antibody (FAB2148P, R&D Systems, PE, diluted 1:10) or *mLDLR* (FAB2255P, R&D Systems, PE, diluted 1:10) for 20 min at 4°C.

Data analysis was performed using FCS Express 6 software.

RNA extraction and ddPCR

Murine livers were stored at −80°C in an RLT+ buffer (Qiagen) solution. 300 µL of RLT+ was added to every 25-mg tissue piece. In the case of cells, 250 µL of RLT+ was added by default. Organs were homogenized using gentleMACS M Tubes (MACS Miltenyi Biotec, 130096335). Tubes were inserted in gentleMACS Octo Dissociator (Miltenyi Biotec), and the protocol selected was gentleMACS program RNA_02, suggested for frozen tissues. Homogenized tissues were subsequently loaded into Maxwell RSC simplyRNA tissue cartridges, and RNA was extracted using the simplyRNA tissue method. Cellular RNA was extracted using an RNeasy+ mini kit (Qiagen), following the manufacturer's instructions. DNA was digested on columns through RNase-Free DNase Set (Qiagen). Reverse transcription was obtained using the SuperScript IV VILO kit (11766050; Thermo Fisher Scientific). LV gene expression was assessed by ddPCR starting from 10 to 25 ng of template cDNA using a primers/probe set designed on wpre or LDLR sequence. HPRT was used as a reference gene (dMmuCPE5095493, Bio-Rad). The PCR reaction was performed with each primer (900 nM) and the probe (250 nM) following the manufacturer's instructions (Bio-Rad), read with a QX200 reader, and analyzed with QuantaSoft software (Bio-Rad). Custom primers and probes, designed and used, were the following.

- *Wpre** Fw: 5′- GGCTGTTGGGCACTGACAAT -3′
- *Wpre** Rv: 5′- ACGTCCCGCGCAGAATC -3′
- *Wpre** Pr 5'-(FAM)- TTTCCATGGCTGCTCGCCTGTGT -(MGB)-3′
- *Ldlr* Fw: 5′- CCATCCTGGCTTCGGCAA -3′
- *Ldlr* Rv: 5′- AGGAACTGGCGGCTGAAG -3′
- *Ldlr* Pr: 5′-FAM- GAGCTCGTCCTCTGTGGTCT -(MGB)-3′
- *co.Ldlr* Fw: 5′- GTAGCCATCCTGAGACCTGC -3′
- *co.Ldlr* Rv: 5′- GCTGTGGAGGAATTGGAGAC -3′
- *co.Ldlr* Pr: 5′-FAM- GATGTGCAGCTCGTCCTCTG -(MGB)-3′

Frk gene expression was determined using an ad hoc ddPCR (QX200 EvaGreen Digital PCR Supermix, Bio-Rad), starting from 10 to 25 ng of template cDNA. Two sets of primers were designed, within the junction between exon 1 and exon 2, or the junction between exon 5 and exon 6, respectively. HPRT was used as a normalizer. The reaction was read with a QX200 reader and analyzed with QuantaSoft software (Bio-Rad). Custom primers, designed and used, were the following.

- *Frk* exon 1–2 Fw: CTTCCAATTACGTGGCGGAG
- *Frk* exon 1–2 Rv: GCCCGTCTGGTTTTCTGAAT
- *Frk* exon 5–6 Fw: GTTGATGAGACATGGAAGCC
- *Frk* exon 5–6 Rv: CGCCATGTCTACCTGTTGAA
- *Hprt* Fw: 5′- GTCGTGATTAGCGATGATGA -3′
- *Hprt* Rv: 5' – CCAAATCCTCGGCATAATGA -3′

For aberrant transcripts assessment, the starting material was ∼150 ng of template cDNA. The following couples of primers were used:

- *LDLR* on LV Fw: GAACTGGCGGCTTAAGAACA
- *Frk* Exon 4 Rv: CAAAAGGGGTTGGTACCTGG

For antisense-oriented LV, the following couples of primers were used.

- *co.Ldlr* on LV Fw: GTCCATCTTCTTTCCCATCG
- *Ldlr* on LV Fw: GCTGAAGAACATCAACAGCA
- *Frk* Exon 4 Rv: CAAAAGGGGTTGGTACCTGG
- *Frk* Exon 5 Rv: CAGGAAGTCATTTGGATCCA

Single bands obtained were then purified with a QIAquick PCR purification Kit (Cat. No. 28106). Reconstitution of aberrant transcript was obtained through Sanger sequencing (Eurofins).

Mouse experiments

C57BL/6 mice were purchased from Jackson Laboratories (stock #000664). B6;129S-LdlrTm1Her/J mice (indicated as $Ldlr^{-/-}$ or LDLR KO) were obtained from Jackson Laboratories (stock #002207). All mice were kept in specific pathogen-free conditions. LV was administered in juvenile mice (2 weeks of age) through retro-orbital plexus (100–200 µL/mouse). Mice were bled from the retro-orbital plexus through capillary tubes. Mice were euthanized by cervical dislocation at the scheduled time. The Institutional Animal Care and Use Committee approved all the procedures performed on mice.

Please cite this article in press as: Canepari et al., Tweaking lentiviral vector design balances efficacy and safety in liver-directed gene therapy for familial hypercholesterolemia, Molecular Therapy (2025), https://doi.org/10.1016/j.ymthe.2025.12.036

Total cholesterol and LDL-c measurements

Mouse blood was centrifuged at 5,500 rpm for 15 min to collect serum and then stored at −80°C. Cholesterol (#0018250540) and LDL-c (#0018256040) were used for the quantitative determination of the serum level with an International Federation of Clinical Chemistry and Laboratory Medicine optimized kinetic ultraviolet method in an ILab650 chemical analyzer (Instrumentation Laboratory) and are expressed as mg/dL. SeraChem Control Level 1 and Level 2 (#0018162412 and #0018162512) were analyzed as quality control.

Aorta and liver collection for histopathological analysis

In experiments where atherosclerosis was evaluated, mice were killed through cervical dislocation and then perfused via the left ventricle with the following solutions at subsequent steps: (i) PBS EDTA (0.5 mM) and (ii) 15 mL PFA (paraformaldehyde, 50 mL). Livers and hearts with aortic arch and thoracic (descending) aorta were collected and fixed in buffered 10% formalin. The aortic arch and descending thoracic aorta were cut and processed. To examine the extent of atherosclerosis in the aortic sinus, the heart was sectioned transversely below the level of the atria as previously described.[55] Sequential 3- to 4-μm sections were cut from the apex toward the base of the heart until the aortic valve leaflets appeared. From this point, at least 20 sections of the aortic root for each animal, representing every second serial section, over a distance of about 250 μm, were taken, stained with hematoxylin and eosin (H&E), and all analyzed. Livers were trimmed, and samples of all four lobes were embedded in two paraffin wax blocks, sectioned, mounted on glass slides, stained with H&E, and analyzed. Macroscopic abnormalities were collected, embedded in paraffin wax, sectioned, mounted on glass slides, stained with H&E, and analyzed. Histopathological changes were graded on a scale of 1–5 as minimal (1), mild (2), moderate (3), marked (4), and severe (5); minimal referred to the least extent discernible and marked to the greatest extent possible. The slides were blindly analyzed and independently peer-reviewed by an experienced pathologist, and a consensus was reached on the findings and scores. In experiments where atherosclerosis was not evaluated, mice were killed through cervical dislocation, and livers were collected and processed as previously described, but without perfusion with PFA. Hypertrophy of hepatocytes, present in the majority of mice treated with ET-co.mLDLR-FRK, was annotated with a severity score ranging from 1 to 3 (minimal, mild, and moderate), characterized by enlarged and vacuolated hepatocytes graded as follows: grade 1, minimal, occasional affected hepatocytes; grade 2, mild, discrete clusters of affected hepatocytes; and grade 3, moderate, multifocal, large clusters of affected hepatocytes. Immunohistochemistry with anti-Ki67 (SP6 Thermo Scientific; rabbit monoclonal 1:100, antigen retrieval with Tris-EDTA pH 9.0, 30 min at 97°C) and anti-CD68 (ABCAM, EPR23917-164, rabbit monoclonal 1:100, antigen retrieval with Tris-EDTA pH 9.0, 30 min at 97°C) was performed on representative liver samples to evaluate the rate of proliferation of hepatocytes and Kupffer cells, respectively. Regarding the Ki67, for each mouse, 10 high-power fields at 200× magnification were randomly evaluated on sections of liver. The mean of Ki67-positive hepatocytes for each mouse, followed by the mean of pooled Ki67-positive hepatocytes per group, was calculated. In the experiment where oil red O staining was performed, a liver sample was placed in optimal cutting temperature (OCT) compound (Killik, Bio-Optica) and snap frozen using isopentane precooled in liquid nitrogen. Then, 5-μm sections were cut and processed according to manufacturing instructions (oil red O, Bio-Optica, 04–220923). The slides were blindly analyzed and independently peer-reviewed by an experienced pathologist, and a consensus was reached on the findings and scores.

Dietary regimen

From 4 weeks of age, all mice were fed *ad libitum* with VRF1 (P) by Special Diet Services. Mice were fed *ad libitum* with Envigo TD.88137 (0.2% total cholesterol) for 3 months, for the WD challenge. After that, they were put back on VRF1.

Immunofluorescence imaging

Livers were harvested from mice, washed with PBS, and fixed for 4 h in PBS 4% paraformaldehyde (PFA) and then washed again in PBS before storage for at least 24 h in 30% sucrose 0.02% sodium azide in H_2O. Livers were then frozen in OCT compound (Killik, Bio-Optica), and slices 5-μm thick were cut at cryostat (Histo-line MC5050), placed on Superfrost Plus microscope slides (Thermo Scientific) and stored at −80°C. All the staining steps were performed protected from lights to preserve endogenous fluorescence. Slides were thawed at room temperature for at least 2 h and then washed three times for 5 min in PBS 0.1% X-Triton. Edges were drawn around the tissue using an immunostaining pap pen (Sigma-Aldrich) to contain staining solutions. The blocking step was performed using PBS 0.1% X-Triton 1% bovine serum albumin (BSA) 5% FBS for 1 h at room temperature in a humid chamber. The blocking solution was then substituted with a mix containing primary antibodies in the blocking solution and incubation lasted 12–16 h at 4°C in a humid chamber. The primary antibodies mix solution was removed, and slides were washed three times for 5 min in PBS 0.1% X-Triton. Secondary antibodies were diluted in the blocking solution with Hoechst (Invitrogen, 1:20,000) and incubated for 1 h at room temperature in a humid chamber. Slides were then washed in PBS, and a cover slip was added using Fluoromount-G (Invitrogen) as a mounting medium. Slides were dried for 16 h at room temperature or longer at 4°C and stored at 4°C before acquisition. The following antibodies were used for immunofluorescence staining: anti-mLDLR rabbit, monoclonal (Thermo Fisher MA5 29725, 1:500), anti-Rabbit IgG Alexa Fluor (AF)647 donkey, polyclonal (Invitrogen, 1:1,000). Images were acquired using confocal microscope Leica TCS SP5, Leica TCS SP8, or Mavig Rs-G4 at 20× or 40× magnification. Images were analyzed using ImageJ or MATLAB software. A custom-written MATLAB pipeline was used to analyze the images, as previously described.[56] Briefly, the positive area was identified by background subtraction and then by applying a fixed threshold. The total liver area was measured by saturating signals from the whole tissue. An additional filter on the dimension ensures the discard of unreasonably small or large objects. The whole tissue is

also segmented through a very low threshold detecting autofluorescence; unwanted areas like fringed borders are manually excluded. Two images were acquired per mouse.

Integration site analysis

ISs were retrieved by Sonication Linker Mediated (SLiM)-PCR as described[57] with minor modifications. Briefly, each sample was processed in technical triplicates using 100 ng of gDNA. DNA shearing was performed using the Covaris E220 Ultrasonicator, generating fragments with an average size of 1,000 bp. The fragmented DNAs were subjected to end repair and 3′ adenylation and then ligated to linker cassettes containing an 8-nucleotide sequence barcode used for sample identification, and all the sequences required for the Read 2 paired-end sequencing. The ligation products were subjected to 35 cycles of exponential PCR using primers specific for the LV LTR and the Linker cassette. A subsequent amplification with additional 10 PCR cycles was performed using a primer specific for the linker cassette and the LTR. These primers contain an 8-nucleotide barcode used for sample identification (coupled with the barcode on the linker cassette) and the sequences needed for the Read 1 sequencing, with additional 12-random-nucleotides allowing easier cluster recognition in the first sequencing cycles in the next-generation sequencing (NGS). The generated SLiM-PCR products are thus associated with a unique pair of barcodes, assembled into libraries, and subjected to NGS Illumina sequencing. Sequencing reads were processed using a custom bioinformatics pipeline (VISPA2)[58] that isolates genomic sequences flanking the vector LTR and maps them to the murine genome (mm9). Because vector integration in the same genomic position in different cells is a very low probability event, identical ISs in independent samples were considered contamination or amplification artifacts, which may occur during the technical procedure. Datasets were pruned from potential contaminations and false positives between each primary mouse and from ISs deriving from unrelated secondary mice. The identical ISs shared between mice belonging to different experimental groups were reassigned based on the identification of the IS by at least two SLiM technical replicates and sequence count numbers. Downstream analyses of vector ISs, such as relative abundance analysis, sharing analysis, and common IS analysis, were performed using ISAnalytics.[59] Clonal abundance estimates as the relative percentage of genome numbers were determined by the R package "sonicLength."[60] A detailed report and source code for ISAnalytics are available at Github: https://github.com/calabrialab/Code_LV_FH.

RNA sequencing

Healthy liver tissues and liver masses were sent to Azenta for RNA extraction, library preparation, and sequencing (Illumina NovaSeq platform, paired-end reads, 2 × 150 bp). Five biological replicates were analyzed for each condition, except for the tumor group, which included six out of seven samples due to one failed sequencing run, resulting in an average of 40.5 ± 7.7 million paired-end reads per sample. Raw sequencing reads were assessed for quality using FastQC (v0.11.6), and low-quality bases and adapter sequences were removed using Trim Galore (v0.6.6). Cleaned reads were aligned to the *Mus musculus* reference genome (GRCm39) using STAR (v2.7.6a) with default parameters. Gene-level read counts were quantified with the featureCounts function from the Subread package (v2.0.1). Differential expression analysis was performed in R using the DESeq2 package (v1.30.0). Library size normalization was performed using DESeq2's median-of-ratios method. p values were corrected for multiple testing using the FDR, and genes with FDR <0.05 and absolute log2 fold change (|log2FC|) >0.5 were considered differentially expressed. Gene set enrichment analysis was performed in R using the enricher function from the clusterProfiler package (v4.7.1.002), with the *Mus musculus* MSigDB Hallmark gene sets as the reference database. Only enriched terms with adjusted p value >0.05 were displayed. For visualization of gene expression of *Frk* and *Mki67* across conditions, normalized counts were obtained using the rlogTransformation function in DESeq2.

Statistical analysis

Statistical analyses were performed upon consulting with professional statisticians at the San Raffaele University Center for Statistics in the Biomedical Sciences (CUSSB). When normality assumptions were not met, non-parametric statistical tests were performed. A two-tailed Mann-Whitney test was performed to compare two independent groups. In the presence of more than two independent groups, the Kruskal-Wallis test followed by post hoc analysis (Dunn's test for multiple comparisons with Bonferroni's correction) was applied. To model the dynamics of transgene amounts over time, properly accounting for dependencies induced by repeated-measures design, linear-mixed effects (LME) models were estimated, specifying random-effect terms on experimental units or sessions. Various transformations of the outcome variable, including logarithmic and ordered quantile normalization, were considered, to fulfill underlying model assumptions. Following the estimation of LME models, post hoc analysis was conducted allowing for pairwise comparison of treatment groups at the last time point. p values were adjusted using Bonferroni's approach, to account for the multiplicity issue. LME models were estimated using R software (version 4.3.1). In all the analyses, the significance threshold was set at 0.05. Inferential techniques were applied in the presence of adequate sample sizes ($n \geq 5$); otherwise, only descriptive statistics are reported.

DATA AVAILABILITY

The LV and reagents described in this manuscript are available to interested scientists upon signing an MTA with standard provisions. RNA-seq data are deposited in GEO (GSE315905). The script for the RNA-seq analysis is available at Gitlab: http://www.bioinfotiget.it/gitlab/custom/Canepari_FH_2025.

ACKNOWLEDGMENTS

This work was supported by the EU Horizon 2020 Program (825825 UPGRADE) and Fondazione Telethon SR-Tiget Core Grant TTACC0422TT. We thank the Advanced Light and Electron Microscopy Bioimaging Center (ALEMBIC, San Raffaele Scientific Institute) for imaging techniques and analysis and Micol Ravà and Leonardo Giustini for cholesterol and LDL-c assessment. We thank E. Barbon for the critical reading of the manuscript. We thank Luigi Naldini and all the members of the Cantore laboratory for helpful discussions. C.C. conducted this study as a partial fulfillment of his International Ph.D. Course in Molecular Medicine at San Raffaele University, Milan.

AUTHOR CONTRIBUTIONS

C.C. designed and performed experiments, analyzed and interpreted data, and wrote the manuscript. M. Milani and F. Starinieri performed experiments, analyzed data, and edited the manuscript. M. Monti performed bioinformatic analyses and edited the manuscript. M.V. performed LV IS analysis and edited the manuscript. A.F., M.C., M.B., L.O., F.G., M.L., and F.R. provided technical support. M.R. and R.N. provided technical support related to histopathology analysis. C.B. and F.C. performed statistical analyses. P.C. supported histopathology analysis and edited the manuscript. E.M. supervised LV IS analysis. S.B. supervised bioinformatic analyses. S.D. and F. Sanvito performed histopathology analysis and edited the manuscript. A.C. supervised and coordinated research, interpreted data, and wrote the manuscript.

DECLARATION OF INTERESTS

C.C. and A.C. are inventors on patent applications submitted by Fondazione Telethon, San Raffaele Scientific Institute, on LV technology related to the work presented in this manuscript. Fondazione Telethon and San Raffaele Scientific Institute, through SR-Tiget, have established a research collaboration on liver-directed lentiviral gene therapy of inherited metabolic disorders with GeneSpire. A.C. is a co-founder and consultant of GeneSpire.

SUPPLEMENTAL INFORMATION

Supplemental information can be found online at https://doi.org/10.1016/j.ymthe.2025.12.036.

REFERENCES

1. Tromp, T.R., Hartgers, M.L., Hovingh, G.K., Vallejo-Vaz, A.J., Ray, K.K., Soran, H., Freiberger, T., Bertolini, S., Harada-Shiba, M., Blom, D.J., et al. (2022). Worldwide experience of homozygous familial hypercholesterolaemia: retrospective cohort study. Lancet *399*, 719–728. https://doi.org/10.1016/S0140-6736(21)02001-8.

2. Brown, M.S., and Goldstein, J.L. (1974). Familial hypercholesterolemia: defective binding of lipoproteins to cultured fibroblasts associated with impaired regulation of 3-hydroxy-3-methylglutaryl coenzyme A reductase activity. Proc. Natl. Acad. Sci. USA *71*, 788–792. https://doi.org/10.1073/pnas.71.3.788.

3. Cuchel, M., Raal, F.J., Hegele, R.A., Al-Rasadi, K., Arca, M., Averna, M., Bruckert, E., Freiberger, T., Gaudet, D., Harada-Shiba, M., et al. (2023). 2023 Update on European Atherosclerosis Society Consensus Statement on Homozygous Familial Hypercholesterolaemia: new treatments and clinical guidance. Eur. Heart J. *44*, 2277–2291. https://doi.org/10.1093/eurheartj/ehad197.

4. Innerarity, T.L., Weisgraber, K.H., Arnold, K.S., Mahley, R.W., Krauss, R.M., Vega, G.L., and Grundy, S.M. (1987). Familial defective apolipoprotein B-100: low density lipoproteins with abnormal receptor binding. Proc. Natl. Acad. Sci. USA *84*, 6919–6923. https://doi.org/10.1073/pnas.84.19.6919.

5. Abifadel, M., Varret, M., Rabès, J.P., Allard, D., Ouguerram, K., Devillers, M., Cruaud, C., Benjannet, S., Wickham, L., Erlich, D., et al. (2003). Mutations in PCSK9 cause autosomal dominant hypercholesterolemia. Nat. Genet. *34*, 154–156. https://doi.org/10.1038/ng1161.

6. Sturm, A.C., Knowles, J.W., Gidding, S.S., Ahmad, Z.S., Ahmed, C.D., Ballantyne, C.M., Baum, S.J., Bourbon, M., Carrié, A., Cuchel, M., et al. (2018). Clinical Genetic Testing for Familial Hypercholesterolemia: JACC Scientific Expert Panel. J. Am. Coll. Cardiol. *72*, 662–680. https://doi.org/10.1016/j.jacc.2018.05.044.

7. Canepari, C., and Cantore, A. (2023). Gene transfer and genome editing for familial hypercholesterolemia. Front. Mol. Med. *3*, 1140997. https://doi.org/10.3389/fmmed.2023.1140997.

8. Anguela, X.M., and High, K.A. (2024). Hemophilia B and gene therapy: a new chapter with etranacogene dezaparvovec. Blood Adv. *8*, 1796–1803. https://doi.org/10.1182/bloodadvances.2023010511.

9. Samelson-Jones, B.J., Small, J.C., and George, L.A. (2024). Roctavian Gene Therapy for Hemophilia A. Blood Adv. *8*, 5179–5189. https://doi.org/10.1182/bloodadvances.2023011847.

10. Somanathan, S., Jacobs, F., Wang, Q., Hanlon, A.L., Wilson, J.M., and Rader, D.J. (2014). AAV vectors expressing LDLR gain-of-function variants demonstrate increased efficacy in mouse models of familial hypercholesterolemia. Circ. Res. *115*, 591–599. https://doi.org/10.1161/CIRCRESAHA.115.304008.

11. Greig, J.A., Limberis, M.P., Bell, P., Chen, S.J., Calcedo, R., Rader, D.J., and Wilson, J.M. (2017). Nonclinical Pharmacology/Toxicology Study of AAV8.TBG.mLDLR and AAV8.TBG.hLDLR in a Mouse Model of Homozygous Familial Hypercholesterolemia. Hum. Gene Ther. Clin. Dev. *28*, 28–38. https://doi.org/10.1089/humc.2017.007.

12. Greig, J.A., Limberis, M.P., Bell, P., Chen, S.J., Calcedo, R., Rader, D.J., and Wilson, J.M. (2017). Non-Clinical Study Examining AAV8.TBG.hLDLR Vector-Associated Toxicity in Chow-Fed Wild-Type and LDLR(+/-) Rhesus Macaques. Hum. Gene Ther. Clin. Dev. *28*, 39–50. https://doi.org/10.1089/humc.2017.014.

13. Wang, L., Muthuramu, I., Somanathan, S., Zhang, H., Bell, P., He, Z., Yu, H., Zhu, Y., Tretiakova, A.P., and Wilson, J.M. (2021). Developing a second-generation clinical candidate AAV vector for gene therapy of familial hypercholesterolemia. Mol. Ther. Methods Clin. Dev. *22*, 1–10. https://doi.org/10.1016/j.omtm.2021.04.017.

14. Milani, M., Annoni, A., Moalli, F., Liu, T., Cesana, D., Calabria, A., Bartolaccini, S., Biffi, M., Russo, F., Visigalli, I., et al. (2019). Phagocytosis-shielded lentiviral vectors improve liver gene therapy in nonhuman primates. Sci. Transl. Med. *11*, eaav7325. https://doi.org/10.1126/scitranslmed.aav7325.

15. Milani, M., Canepari, C., Liu, T., Biffi, M., Russo, F., Plati, T., Curto, R., Patarroyo-White, S., Drager, D., Visigalli, I., et al. (2022). Liver-directed lentiviral gene therapy corrects hemophilia A mice and achieves normal-range factor VIII activity in non-human primates. Nat. Commun. *13*, 2454. https://doi.org/10.1038/s41467-022-30102-3.

16. Nicolas, C.T., VanLith, C.J., Hickey, R.D., Du, Z., Hillin, L.G., Guthman, R.M., Cao, W.J., Haugo, B., Lillegard, A., Roy, D., et al. (2022). In vivo lentiviral vector gene therapy to cure hereditary tyrosinemia type 1 and prevent development of precancerous and cancerous lesions. Nat. Commun. *13*, 5012. https://doi.org/10.1038/s41467-022-32576-7.

17. Canepari, C., Milani, M., Simoni, C., Starinieri, F., Volpin, M., Fabiano, A., Biffi, M., Russo, F., Norata, R., Rocchi, M., et al. (2025). Enhancing the potency of in vivo lentiviral vector mediated gene therapy to hepatocytes. Nat. Commun. *16*, 4802. https://doi.org/10.1038/s41467-025-60073-0.

18. Cantore, A., Ranzani, M., Bartholomae, C.C., Volpin, M., Valle, P.D., Sanvito, F., Sergi, L.S., Gallina, P., Benedicenti, F., Bellinger, D., et al. (2015). Liver-directed lentiviral gene therapy in a dog model of hemophilia B. Sci. Transl. Med. *7*, 277ra28. https://doi.org/10.1126/scitranslmed.aaa1405.

19. Finkelshtein, D., Werman, A., Novick, D., Barak, S., and Rubinstein, M. (2013). LDL receptor and its family members serve as the cellular receptors for vesicular stomatitis virus. Proc. Natl. Acad. Sci. USA *110*, 7306–7311. https://doi.org/10.1073/pnas.1214441110.

20. Nikolic, J., Belot, L., Raux, H., Legrand, P., Gaudin, Y., and A Albertini, A. (2018). Structural basis for the recognition of LDL-receptor family members by VSV glycoprotein. Nat. Commun. *9*, 1029. https://doi.org/10.1038/s41467-018-03432-4.

21. Al-Allaf, F.A., Coutelle, C., Waddington, S.N., David, A.L., Harbottle, R., and Themis, M. (2010). LDLR-Gene therapy for familial hypercholesterolaemia: problems, progress, and perspectives. Int. Arch. Med. *3*, 36. https://doi.org/10.1186/1755-7682-3-36.

22. Otahal, A., Fuchs, R., Al-Allaf, F.A., and Blaas, D. (2015). Release of Vesicular Stomatitis Virus Spike Protein G-Pseudotyped Lentivirus from the Host Cell Is Impaired upon Low-Density Lipoprotein Receptor Overexpression. J. Virol. *89*, 11723–11726. https://doi.org/10.1128/JVI.01869-15.

23. Kankkonen, H.M., Vähäkangas, E., Marr, R.A., Pakkanen, T., Laurema, A., Leppänen, P., Jalkanen, J., Verma, I.M., and Ylä-Herttuala, S. (2004). Long-term lowering of plasma cholesterol levels in LDL-receptor-deficient WHHL rabbits by gene therapy. Mol. Ther. *9*, 548–556. https://doi.org/10.1016/j.ymthe.2004.01.015.

24. Hytonen, E., Laurema, A., Kankkonen, H., Miyanohara, A., Karja, V., Hujo, M., Laham-Karam, N., and Yla-Herttuala, S. (2019). Bile-duct proliferation as an unexpected side-effect after AAV2-LDLR gene transfer to rabbit liver. Sci. Rep. *9*, 6934. https://doi.org/10.1038/s41598-019-43459-1.

25. Zanta-Boussif, M.A., Charrier, S., Brice-Ouzet, A., Martin, S., Opolon, P., Thrasher, A.J., Hope, T.J., and Galy, A. (2009). Validation of a mutated PRE sequence allowing high and sustained transgene expression while abrogating WHV-X protein synthesis: application to the gene therapy of WAS. Gene Ther. *16*, 605–619. https://doi.org/10.1038/gt.2009.3.

26. Schambach, A., Bohne, J., Baum, C., Hermann, F.G., Egerer, L., von Laer, D., and Giroglou, T. (2006). Woodchuck hepatitis virus post-transcriptional regulatory element deleted from X protein and promoter sequences enhances retroviral vector titer and expression. Gene Ther. *13*, 641–645. https://doi.org/10.1038/sj.gt.3302698.

27. Brown, B.D., Cantore, A., Annoni, A., Sergi, L.S., Lombardo, A., Della Valle, P., D'Angelo, A., and Naldini, L. (2007). A microRNA-regulated lentiviral vector mediates stable correction of hemophilia B mice. Blood *110*, 4144–4152. https://doi.org/10.1182/blood-2007-03-078493.

28. Schauber, C.A., Tuerk, M.J., Pacheco, C.D., Escarpe, P.A., and Veres, G. (2004). Lentiviral vectors pseudotyped with baculovirus gp64 efficiently transduce mouse cells in vivo and show tropism restriction against hematopoietic cell types in vitro. Gene Ther. *11*, 266–275. https://doi.org/10.1038/sj.gt.3302170.

29. Milani, M., Canepari, C., Assanelli, S., Merlin, S., Borroni, E., Starinieri, F., Biffi, M., Russo, F., Fabiano, A., Zambroni, D., et al. (2024). GP64-pseudotyped lentiviral vectors target liver endothelial cells and correct hemophilia A mice. EMBO Mol. Med. *16*, 1427–1450. https://doi.org/10.1038/s44321-024-00072-8.

30. Kassim, S.H., Li, H., Bell, P., Somanathan, S., Lagor, W., Jacobs, F., Billheimer, J., Wilson, J.M., and Rader, D.J. (2013). Adeno-associated virus serotype 8 gene therapy leads to significant lowering of plasma cholesterol levels in humanized mouse models of homozygous and heterozygous familial hypercholesterolemia. Hum. Gene Ther. *24*, 19–26. https://doi.org/10.1089/hum.2012.108.

31. Emini Veseli, B., Perrotta, P., De Meyer, G.R.A., Roth, L., Van der Donckt, C., Martinet, W., and De Meyer, G.R.Y. (2017). Animal models of atherosclerosis. Eur. J. Pharmacol. *816*, 3–13. https://doi.org/10.1016/j.ejphar.2017.05.010.

32. Homer, V.M., Marais, A.D., Charlton, F., Laurie, A.D., Hurndell, N., Scott, R., Mangili, F., Sullivan, D.R., Barter, P.J., Rye, K.A., et al. (2008). Identification and characterization of two non-secreted PCSK9 mutants associated with familial hypercholesterolemia in cohorts from New Zealand and South Africa. Atherosclerosis *196*, 659–666. https://doi.org/10.1016/j.atherosclerosis.2007.07.022.

33. Pilati, C., Letouzé, E., Nault, J.C., Imbeaud, S., Boulai, A., Calderaro, J., Poussin, K., Franconi, A., Couchy, G., Morcrette, G., et al. (2014). Genomic profiling of hepatocellular adenomas reveals recurrent FRK-activating mutations and the mechanisms of malignant transformation. Cancer Cell *25*, 428–441. https://doi.org/10.1016/j.ccr.2014.03.005.

34. Bayard, Q., Caruso, S., Couchy, G., Rebouissou, S., Bioulac Sage, P., Balabaud, C., Paradis, V., Sturm, N., de Muret, A., Guettier, C., et al. (2020). Recurrent chromosomal rearrangements of ROS1, FRK and IL6 activating JAK/STAT pathway in inflammatory hepatocellular adenomas. Gut *69*, 1667–1676. https://doi.org/10.1136/gutjnl-2019-319790.

35. Cesana, D., Ranzani, M., Volpin, M., Bartholomae, C., Duros, C., Artus, A., Merella, S., Benedicenti, F., Sergi Sergi, L., Sanvito, F., et al. (2014). Uncovering and dissecting the genotoxicity of self-inactivating lentiviral vectors in vivo. Mol. Ther. *22*, 774–785. https://doi.org/10.1038/mt.2014.3.

36. Cesana, D., Sgualdino, J., Rudilosso, L., Merella, S., Naldini, L., and Montini, E. (2012). Whole transcriptome characterization of aberrant splicing events induced by lentiviral vector integrations. J. Clin. Invest. *122*, 1667–1676. https://doi.org/10.1172/JCI62189.

37. Farese, R.V., Jr., Véniant, M.M., Cham, C.M., Flynn, L.M., Pierotti, V., Loring, J.F., Traber, M., Ruland, S., Stokowski, R.S., Huszar, D., and Young, S.G. (1996). Phenotypic analysis of mice expressing exclusively apolipoprotein B48 or apolipoprotein B100. Proc. Natl. Acad. Sci. USA *93*, 6393–6398. https://doi.org/10.1073/pnas.93.13.6393.

38. Simoni, C., Barbon, E., Muro, A.F., and Cantore, A. (2024). In vivo liver targeted genome editing as therapeutic approach: progresses and challenges. Front Genome *6*, 1458037. https://doi.org/10.3389/fgeed.2024.1458037.

39. van der Sluis, R.J., Van Eck, M., and Hoekstra, M. (2015). Adrenocortical LDL receptor function negatively influences glucocorticoid output. J. Endocrinol. *226*, 145–154. https://doi.org/10.1530/JOE-15-0023.

40. Starzl, T.E., Bilheimer, D.W., Bahnson, H.T., Shaw, B.W., Jr., Hardesty, R.L., Griffith, B.P., Iwatsuki, S., Zitelli, B.J., Gartner, J.C., Jr., Malatack, J.J., et al. (1984). Heart-liver transplantation in a patient with familial hypercholesterolaemia. Lancet *1*, 1382–1383. https://doi.org/10.1016/s0140-6736(84)91876-2.

41. Gaudelli, N.M., Komor, A.C., Rees, H.A., Packer, M.S., Badran, A.H., Bryson, D.I., and Liu, D.R. (2017). Programmable base editing of A*T to G*C in genomic DNA without DNA cleavage. Nature *551*, 464–471. https://doi.org/10.1038/nature24644.

42. Komor, A.C., Kim, Y.B., Packer, M.S., Zuris, J.A., and Liu, D.R. (2016). Programmable editing of a target base in genomic DNA without double-stranded DNA cleavage. Nature *533*, 420–424. https://doi.org/10.1038/nature17946.

43. Makhmudova, U., Steinhagen-Thiessen, E., Volpe, M., and Landmesser, U. (2024). Advances in nucleic acid-targeted therapies for cardiovascular disease prevention. Cardiovasc. Res. *120*, 1107–1125. https://doi.org/10.1093/cvr/cvae136.

44. Musunuru, K., Chadwick, A.C., Mizoguchi, T., Garcia, S.P., DeNizio, J.E., Reiss, C.W., Wang, K., Iyer, S., Dutta, C., Clendaniel, V., et al. (2021). In vivo CRISPR base editing of PCSK9 durably lowers cholesterol in primates. Nature *593*, 429–434. https://doi.org/10.1038/s41586-021-03534-y.

45. Cappelluti, M.A., Mollica Poeta, V., Valsoni, S., Quarato, P., Merlin, S., Merelli, I., and Lombardo, A. (2024). Durable and efficient gene silencing in vivo by hit-and-run epigenome editing. Nature *627*, 416–423. https://doi.org/10.1038/s41586-024-07087-8.

46. Naddaf, M. (2023). First trial of 'base editing' in humans lowers cholesterol - but raises safety concerns. Nature *623*, 671–672. https://doi.org/10.1038/d41586-023-03543-z.

47. Poletti, V., and Mavilio, F. (2021). Designing Lentiviral Vectors for Gene Therapy of Genetic Diseases. Viruses *13*, 1526. https://doi.org/10.3390/v13081526.

48. Willer, C.J., Schmidt, E.M., Sengupta, S., Peloso, G.M., Gustafsson, S., Kanoni, S., Ganna, A., Chen, J., Buchkovich, M.L., Mora, S., et al. (2013). Discovery and refinement of loci associated with lipid levels. Nat. Genet. *45*, 1274–1283. https://doi.org/10.1038/ng.2797.

49. Nault, J.C., Couchy, G., Balabaud, C., Morcrette, G., Caruso, S., Blanc, J.F., Bacq, Y., Calderaro, J., Paradis, V., Ramos, J., et al. (2017). Molecular Classification of Hepatocellular Adenoma Associates With Risk Factors, Bleeding, and Malignant Transformation. Gastroenterology *152*, 880–894.e6. https://doi.org/10.1053/j.gastro.2016.11.042.

50. Duncan, C.N., Bledsoe, J.R., Grzywacz, B., Beckman, A., Bonner, M., Eichler, F.S., Kühl, J.S., Harris, M.H., Slauson, S., Colvin, R.A., et al. (2024). Hematologic Cancer after Gene Therapy for Cerebral Adrenoleukodystrophy. N. Engl. J. Med. *391*, 1287–1301. https://doi.org/10.1056/NEJMoa2405541.

51. Calabria, A., Spinozzi, G., Cesana, D., Buscaroli, E., Benedicenti, F., Pais, G., Gazzo, F., Scala, S., Lidonnici, M.R., Scaramuzza, S., et al. (2024). Long-term lineage commitment in hematopoietic stem cell gene therapy. Nature *636*, 162–171. https://doi.org/10.1038/s41586-024-08250-x.

52. Cichon, G., Willnow, T., Herwig, S., Uckert, W., Löser, P., Schmidt, H.H., Benhidjeb, T., Schlag, P.M., Schnieders, F., Niedzielska, D., and Heeren, J. (2004). Non-physiological overexpression of the low density lipoprotein receptor (LDLr) gene in the liver induces pathological intracellular lipid and cholesterol storage. J. Gene Med. *6*, 166–175. https://doi.org/10.1002/jgm.473.

53. Bjornsson, E., Gunnarsdottir, K., Halldorsson, G.H., Sigurdsson, A., Arnadottir, G.A., Jonsson, H., Olafsdottir, E.F., Niehus, S., Kehr, B., Sveinbjörnsson, G., et al. (2021). Lifelong Reduction in LDL (Low-Density Lipoprotein) Cholesterol due to a Gain-of-Function Mutation in LDLR. Circ. Genom. Precis. Med. *14*, e003029. https://doi.org/10.1161/CIRCGEN.120.003029.

54. Ioannou, G.N., Lee, S.P., Linsley, P.S., Gersuk, V., Yeh, M.M., Chen, Y.Y., Peng, Y.J., Dutta, M., Mascarinas, G., Molla, B., et al. (2022). Pcsk9 Deletion Promotes Murine Nonalcoholic Steatohepatitis and Hepatic Carcinogenesis: Role of Cholesterol. Hepatol. Commun. *6*, 780–794. https://doi.org/10.1002/hep4.1858.

55. Cristofori, P., Crivellente, F., Campagnola, M., Pasini, A.F., Garbin, U., Rigoni, A., Tosetti, M., Turton, J., Faustinelli, I., and Cominacini, L. (2004). Reduced progression of atherosclerosis in apolipoprotein E-deficient mice treated with lacidipine is associated with a decreased susceptibility of low-density lipoprotein to oxidation. Int. J. Exp. Pathol. *85*, 105–114. https://doi.org/10.1111/j.0959-9673.2004.00375.x.

56. Milani, M., Starinieri, F., Beretta, S., Monti, M., Canepari, C., Marabotti, F., Zambrano, S., Mazza, D., Fabiano, A., Simoni, C., et al. (2025). Spatiotemporal liver dynamics shape hepatocellular heterogeneity and impact in vivo gene engineering. J. Hepatol. *83*, 1392–1409. https://doi.org/10.1016/j.jhep.2025.06.018.

57. Cesana, D., Calabria, A., Rudilosso, L., Gallina, P., Benedicenti, F., Spinozzi, G., Schiroli, G., Magnani, A., Acquati, S., Fumagalli, F., et al. (2021). Retrieval of vector integration sites from cell-free DNA. Nat. Med. *27*, 1458–1470. https://doi.org/10.1038/s41591-021-01389-4.

58. Spinozzi, G., Calabria, A., Brasca, S., Beretta, S., Merelli, I., Milanesi, L., and Montini, E. (2017). VISPA2: a scalable pipeline for high-throughput identification and annotation of vector integration sites. BMC Bioinformatics *18*, 520. https://doi.org/10.1186/s12859-017-1937-9.

59. Pais, G., Spinozzi, G., Cesana, D., Benedicenti, F., Albertini, A., Bernardo, M.E., Gentner, B., Montini, E., and Calabria, A. (2023). ISAnalytics enables longitudinal and high-throughput clonal tracking studies in hematopoietic stem cell gene therapy applications. Brief. Bioinform. *24*, bbac551. https://doi.org/10.1093/bib/bbac551.

60. Berry, C.C., Gillet, N.A., Melamed, A., Gormley, N., Bangham, C.R.M., and Bushman, F.D. (2012). Estimating abundances of retroviral insertion sites from DNA fragment length data. Bioinformatics *28*, 755–762. https://doi.org/10.1093/bioinformatics/bts004.